UNIVERSIDADE ESTADUAL DE CAMPINAS

Instituto de Física Gleb Wataghin

Pedro de Asevedo Piquet Carneiro

An EEG-based brain functional connectivity investigation of previously injured footballers

Investigação da conectividade funcional cerebral baseada em EEG em jogadores de futebol previamente lesionados

CAMPINAS

2024

PEDRO DE ASEVEDO PIQUET CARNEIRO

An EEG-based brain functional connectivity investigation of previously injured footballers

Investigação da conectividade funcional cerebral baseada em EEG em jogadores de futebol previamente lesionados

Dissertation presented to the Gleb Wataghin Physics Institute of the University of Campinas in partial fulfillment of the requirements for the degree of Master in Physics, in the area of Applied Physics.

Dissertação apresentada ao Instituto de Física Gleb Wataghin da Universidade Estadual de Campinas como parte dos requisitos exigidos para a obtenção do título de Mestre em Física, na área de Física Aplicada.

Supervisor/Orientadora: Profa. Dra. GABRIELA CASTELLANO

ESTE EXEMPLAR CORRESPONDE À
VERSÃO FINAL TESE DEFENDIDA PELO
ALUNO PEDRO DE ASEVEDO PIQUET CARNEIRO,
E ORIENTADA PELA PROFA. DRA. GABRIELA
CASTELLANO.

CAMPINAS
2024

Ficha catalográfica
Universidade Estadual de Campinas (UNICAMP)
Biblioteca do Instituto de Física Gleb Wataghin
Lucimeire de Oliveira Silva da Rocha - CRB 8-9174

Carneiro, Pedro de Asevedo Piquet, 1998-
C215e An EEG-based brain functional connectivity investigation of previously injured footballers / Pedro de Asevedo Piquet Carneiro. – Campinas, SP : [s.n.], 2024.

Orientador: Gabriela Castellano.
Dissertação (mestrado) – Universidade Estadual de Campinas (UNICAMP), Instituto de Física Gleb Wataghin.

1. Eletroencefalografia. 2. Conectividade funcional. 3. Lesões nos isquiotibiais. I. Castellano, Gabriela, 1970-. II. Universidade Estadual de Campinas (UNICAMP). Instituto de Física Gleb Wataghin. III. Título.

Informações complementares

Título em outro idioma: Investigação da conectividade funcional cerebral baseada em EEG em jogadores de futebol previamente lesionados
Palavras-chave em inglês:
Electroencephalography
Functional connectivity
Hamstring injuries
Área de concentração: Física Aplicada
Titulação: Mestre em Física
Banca examinadora:
Gabriela Castellano [Orientador]
José Antônio Brum
Marco Carlos Uchida
Data de defesa: 18-12-2024
Programa de Pós-Graduação: Física

Identificação e informações acadêmicas do(a) aluno(a)
- ORCID do autor: https://orcid.org/0000-0001-6948-4531
- Currículo Lattes do autor: http://lattes.cnpq.br/7454332042603069

MEMBROS DA COMISSÃO EXAMINADORA DA DISSERTAÇÃO DE MESTRADO DO ALUNO PEDRO DE ASEVEDO PIQUET CARNEIRO - RA 223251, APRESENTADA E APROVADA AO INSTITUTO DE FÍSICA GLEB WATAGHIN, DA UNIVERSIDADE ESTADUAL DE CAMPINAS, EM 18/12/2024.

COMISSÃO JULGADORA:

- Profa. Dra. Gabriela Castellano (IFGW/ UNICAMP) - Presidente e Orientadora

- Prof. Dr. José Antônio Brum (IFGW/ UNICAMP)

- Prof. Dr. Marco Carlos Uchida (FEF/ UNICAMP)

OBS.: Ata da defesa com as respectivas assinaturas dos membros encontra-se no SIGA/Sistema de Fluxo de Dissertação/Tese e na Secretaria do Programa da Unidade.

CAMPINAS

2024

ACKNOWLEDGEMENTS

First and foremost, I am deeply grateful to my family for the unwavering and continuous support throughout every single step in my academic career and personal life. My parents, Rosângela and Marcelo, have always been a constant source of nothing but encouragement, never once casting doubt on my goals, no matter how ambitious they were. To my sister Lara, who, through our differences, has taught me invaluable lessons about seeing the world from another perspective. I owe my deepest appreciation to my grandparents, Rosélia and Bernardo, who stand as living examples of unrelenting dedication to their respective crafts, one I could only hope to achieve in my own path. And last, but definitely not least, I am profoundly grateful for all the wonderfully insightful conversations I've had with my uncle Leandro, as each one of them helped shape the scientist I am today.

I am deeply grateful to all my dear friends, those who have been with me from the beginning and those who joined along the way. Each of whom, in their own unique way, has provided me with the strength and countless reasons to always keep on going.

I would like to extend my thanks to the academic advisors that have accompanied me in my journey. Firstly, to Ryan Draft, who has been a guiding presence since the summer of 2019, consistently showing immense interest in my academic path and always making himself available to discuss whatever was on my mind. To my supervisor Gabriela Castellano, for the support throughout both my undergraduate and master's thesis. Thank you for providing your students an example of professionalism and dedication within academia.

I would also like to express my appreciation to our collaborators at Lisboa, José Pedro and Sandro, for providing the data that made this project possible and for the many discussions that have been incorporated into this work.

A special thanks to my psychologist, Isabela, as I probably wouldn't have gotten this far without her.

Finally, a most heartfelt thanks to my dearest scientific correspondent, Bianca McEvoy, who, despite having no obligation whatsoever, has dedicated countless hours to thoroughly reviewing my work, offering extensive feedback, and engaging in the most arduous yet deeply rewarding conversations to help me overcome the many challenges in my research. I am forever in your debt.

"Which is more important," asked the Big Panda, "the journey or the destination?"

"The company." said the Tiny Dragon.

Acknowledgement of funding sources: This research was supported by São Paulo Research Foundation – Brazil (FAPESP) – Grants 2022/14853-4 and 2013/07559-3, and Brazilian National Council for Scientific and Technological Development (CNPq) – Grant 304008/2021-4. This study was financed in part by the Coordenação de Aperfeiçoamento de Pessoal de Nível Superior - Brasil (CAPES) - Finance Code 001.

ABSTRACT

Hamstring strain injuries (HSIs) remain a prevalent concern among professional football players, often leading to long-term implications for sport performance and health. The neuromuscular adaptations following HSIs, particularly within the central nervous system, are still poorly understood. This study investigates the functional brain connectivity changes in previously injured footballers during motor tasks using electroencephalography (EEG). We analyzed the EEG data from 89 male professional football players, 30 of whom had a history of HSIs, acquired during a maximum-speed knee flexion-extension task. A functional connectivity (FC) analysis focusing mainly on the alpha frequency band using weighted phase-lag index (wPLI) was conducted to explore the potential impact of HSIs on brain function during rigorous motor activity. Our findings revealed a significant decrease in global FC in the alpha frequency band during the motor task compared to rest for all participants, indicating a widespread reduction in alpha connectivity associated with motor activity. Notably, players with a history of HSI exhibited a more pronounced decrease in global alpha connectivity during the task, particularly in the frontal and temporal networks. Furthermore, a significant negative correlation was observed between an injury severity index and alpha FC reduction, mainly in the frontal and parietal networks, implying that more severe and more recent injuries lead to greater cortical adaptations. The observed alterations in brain connectivity suggest that footballers with a history of HSI may need to recruit additional cortical resources to maintain motor performance, potentially influencing their overall injury risk and rehabilitation process. This study provides new insights into the possible impact of HSIs on the FC profile during motor activity and it might represent a first step towards using EEG-based connectivity analysis as a tool for developing targeted rehabilitation protocols and injury prevention strategies tailored to the cognitive profile of each athlete.

RESUMO

Lesões por distensão dos isquiotibiais (HSIs) continuam sendo uma preocupação prevalente entre jogadores profissional de futebol, frequentemente levando a implicações de longo prazo para a saúde e desempenho esportivo. As adaptações neuromusculares após HSIs, particularmente dentro do sistema nervoso central, ainda são pouco compreendidas. Este estudo investiga as mudanças na conectividade funcional do cérebro em jogadores de futebol previamente lesionados durante a execução de tarefas motoras, utilizando eletroencefalografia (EEG). Os dados de EEG de 89 jogadores de futebol profissionais do sexo masculino foram analisados, dos quais 30 tinham histórico de HSIs, adquiridos durante uma tarefa de flexão-extensão de joelho em velocidade máxima. Foi conduzida uma análise de conectividade funcional (FC), focando principalmente na banda de frequência alfa usando o índice de defasagem ponderado (wPLI) para explorar o impacto potencial das HSIs na função cerebral durante uma atividade motora rigorosa. Nossos resultados revelaram uma diminuição significativa na conectividade global na banda de frequência alfa durante a execução da tarefa em comparação ao repouso para todos os participantes, indicando uma redução generalizada na conectividade alfa associada à atividade motora. Notavelmente, jogadores com histórico de HSI apresentaram uma diminuição mais acentuada na conectividade global alfa durante a tarefa, particularmente nas redes frontal e temporal. Além disso, foi observada uma correlação negativa significativa entre um índice de gravidade da lesão e a redução da FC alfa, principalmente nas redes frontal e parietal, sugerindo que lesões mais graves e mais recentes levam a maiores adaptações corticais. As alterações observadas na conectividade cerebral sugerem que jogadores de futebol com histórico de HSI podem precisar recrutar recursos corticais adicionais para manter o desempenho motor, potencialmente influenciando seu risco geral de lesão e processo de reabilitação. Este estudo fornece novos insights sobre o possível impacto das HSIs no perfil de FC durante a atividade motora e pode representar um primeiro passo para o uso da análise de conectividade baseada em EEG como uma ferramenta para desenvolver protocolos de reabilitação direcionados e estratégias de prevenção de lesões adaptadas ao perfil cognitivo de cada atleta.

LIST OF FIGURES

LIST OF TABLES

LIST OF ACRONYMS

ACL	Anterior cruciate ligament
CMR	Common mode rejection
CNS	Central nervous system
DTI	Diffusion tensor imaging
ECG	Electrocardiogram
EEG	Electroencephalography
EMG	Electromyography
EOG	Electrooculography
EPSP	Excitatory post-synaptic potential
fMRI	Functional magnetic resonance imaging
fNIRS	Functional near infrared spectroscopy
FC	Functional connectivity
ICA	Independent component analysis
IPSP	Inhibitory post-synaptic potential
LFP	Local field potential
MEG	Magnetoencephalography
PET	Positron emission tomography
PNS	Peripheral nervous system
SNR	Signal-to-noise ratio
HAPPE	Harvard automated processing pipeline for EEG
HSI	Hamstring strain injuries
wPLI	Weighted phase lag index

TABLE OF CONTENTS

1. INTRODUCTION

1.1. Motivation

A collaboration was established between the Neuromuscular Research Lab, Faculty of Human Kinetics, University of Lisboa and the Neurophysics group at the Gleb Wataghin Institute of Physics at the Universidade Estadual de Campinas (UNICAMP) to investigate possible changes in neural activity of previously injured professional football players during the execution of a rigorous motor task. Our role in this project was to thoroughly analyze the provided electroencephalograph (EEG) data using tools from whole brain connectivity analysis.

Although research efforts have increased in recent years, the incidence of hamstring strain injuries (HSIs) continues to grow among professional football players (Ekstrand et al., 2023). This injury is known to negatively impact player and team performance (Drew et al., 2017; Eirale et al., 2013; Hägglund et al., 2013) and to have a high financial cost (Nieto Torrejón et al., 2024). These injuries are defined as a sudden onset of posterior thigh pain during activity which is reproduced with hamstring stretching and/or activation (Martin et al., 2022) which led to training or match time loss (Fuller et al., 2006); and often occur during actions involving fast muscle actions (Jokela et al., 2023).

HSIs also show a high recurrence rate (Ekstrand et al., 2023). However, parameters such as injury severity on physical examination or imaging and strength measurements have shown a poor or uncertain association with recurrence (Heiderscheit et al., 2010). Conversely, persistent neuromuscular inhibition has been strongly suggested to contribute to recurrence (Fyfe et al., 2013; Opar et al., 2012). This inhibition is thought to serve as a protective mechanism to reduce pain and tissue load after injury (Fyfe et al., 2013); however, muscle pain may cause chronic supraspinal adaptations (Graven-Nielsen & Arendt-Nielsen, 2010), affecting the voluntary recruitment ability in the long term (Fyfe et al., 2013). Moreover, Di Trani suggested that HSIs damage mechanoreceptors, leading to post-deafferentation cortical remodeling (Andrea Di Trani, 2017). These cortical changes can significantly impact the integration of proprioceptive/sensory input, which is crucial for muscle control and coordination, especially during actions such as sprinting, which require rapid and accurate adjustments (Roussiez & Van Cant, 2019). This notion is supported by studies indicating that proprioceptive, tactile, and spatial deficits in response to hamstring pain are associated with cortical reorganization in

regions processing lower limb sensory information (Cavaleri et al., 2023; Moukhaiber et al., 2023; Summers et al., 2021); moreover, Australian football athletes with previous HSI have shown impaired joint position sense and leg swing movement discrimination (Cameron et al., 2003). Despite these findings suggestive of post-HSI cortical adaptations across multiple regions, research on the relationship between HSIs and changes in brain activity is scarce. Accordingly, the recent London consensus has highlighted the need for further research on central nervous system (CNS) changes associated with HSIs (Paton et al., 2023). Existing research on EEG adaptations after musculoskeletal injuries does, however, provide encouraging evidence of how these adaptations may also be present in HSIs. Zhang et al. (2022) investigated cortical activity changes in soccer players with chronic ankle instability and found differences in frontal theta but not in alpha power during drop-jump landing compared to healthy controls, suggesting that lower limb joint instability induces band-specific adaptations. Similarly, Baumeister et al. (2008, 2011) studied altered EEG activity after anterior cruciate ligament (ACL) reconstruction during force control and joint position sense tasks and found higher frontal theta power in both tasks and lower parietal alpha power during force reproduction tasks in the affected knee of injured individuals (Baumeister et al., 2008, 2011). These studies highlight the task dependency of cortical activation changes following lower limb injuries, emphasizing the role of theta and alpha oscillations in compensatory neural mechanisms. However, it is important to note that these studies primarily used power analysis and did not specifically examine functional connectivity (FC).

To the best of our knowledge, studies examining brain connectivity in athletes with previous HSI are nonexistent, and those involving other injuries do not assess FC during movement and are based on functional magnetic resonance imaging (fMRI) (Diekfuss et al., 2019, 2020). Brain FC can be assessed with the use of electroencephalography (EEG) through similarities between the neural activity from multiple brain regions, providing information about their synchronization. Applying graph theory to FC allows extraction of essential parameters that depict the underlying brain network characteristics (Bastos & Schoffelen, 2016).

Given the lack of studies relating brain FC to lower limb injuries (including HSIs), the primary objective of this work was to determine whether footballers with and without HSI history show differences in functional brain connectivity during a maximum-speed knee flexion-extension task. We hypothesized that differences in FC metrics would be found between players with and without HSI history, reflecting potential long-term impacts of this injury on brain function. In addition, we explored whether any potential changes would be associated with injury severity

(i.e. time loss due to injury) and the time difference between testing and injury date, considering that the magnitude of the injury and the time between events may influence brain adaptive responses. By addressing these hypotheses, we aim to enhance the understanding of how musculoskeletal injuries can affect brain function and to identify potential biomarkers for injury assessment and rehabilitation.

1.2. Project Overview

As is illustrated in the schematic below (Fig. 1), the project pipeline began with subject selection, clinical data collection and EEG data acquisition, all of which was conducted by our collaborators at the University of Lisbon. Following data collection, EEG signals were preprocessed using standardized techniques, ensuring clean data for analysis. From the processed data, we extracted individual FC matrices, which were then used to construct undirected weighted graphs representing the FC network of each participant. From these graphs, we calculated graph-theoretical metrics, such as degree. These metrics were initially used to perform group comparisons between injured and non-injured players, identifying key connectivity differences across the two groups. Subsequently, we examined correlations between the graph metrics and clinical variables, providing insights into how specific connectivity patterns might be associated with injury severity and recovery.

This thesis is organized into five chapters. Chapter 2 provides a comprehensive overview of the theoretical foundations that support this study. Chapter 3 details the materials and methods, describing the study design, participant recruitment, experimental protocol, and data processing steps. Chapter 4 presents the results obtained from the EEG analysis, highlighting key findings on brain functional connectivity among injured and non-injured footballers. In Chapter 5, these findings are discussed in the context of existing literature, addressing the implications and limitations of the study. Finally, Chapter 6 summarizes the main conclusions and suggests directions for future research.

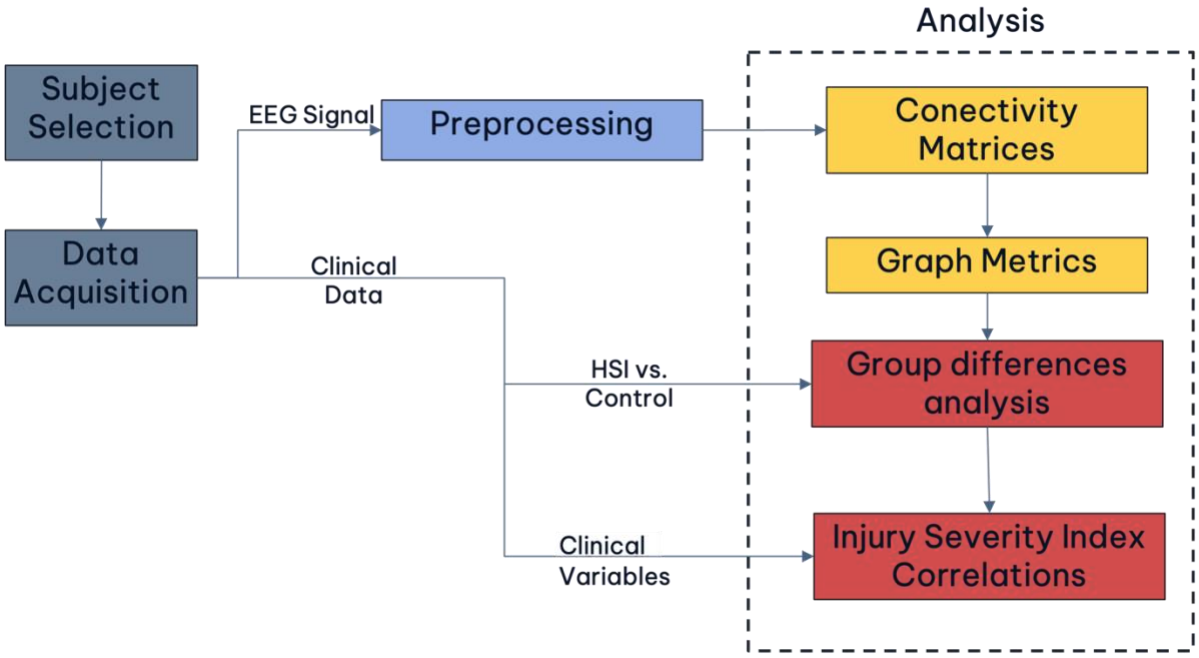

Figure 1. Overview of the entire project pipeline. Workflow schematic illustrating the several steps concluded in order to achieve the results presented in this thesis.

2. THEORETICAL FOUNDATIONS

2.1. The human nervous system

The human nervous system is made up of two parts: The CNS, which consists of two main structures, the brain and the spinal cord; and the peripheral nervous system (PNS), which consists of a large network of nerves that branch out from the spinal cord connecting it to muscles, joints, skin, etc. These connections allow for voluntary motor control, proprioception, as well as the perception of the basic senses via the transmission of efferent motor and afferent sensory signals and stimuli (Haines & Terrell, 2018).

The brain makes up the largest portion of the CNS and is responsible for the perception and processing of incoming sensory stimuli from the PNS, executing voluntary motor responses by transmitting neural signals to nerves in the PNS, and for regulation of homeostatic mechanisms. The brain is separated into three main regions: brainstem, cerebellum and cerebrum (Fig. 2 Left). The brainstem connects the forebrain with the spinal cord and has critical roles in regulating heart and respiratory function, modulating the CNS and the body's sleep cycle (Joynt, 2024). The cerebellum plays an important role in motor control by receiving inputs from sensory systems and from other parts of the brain and integrates these inputs to fine-tune motor activity (Fine et al., 2002).

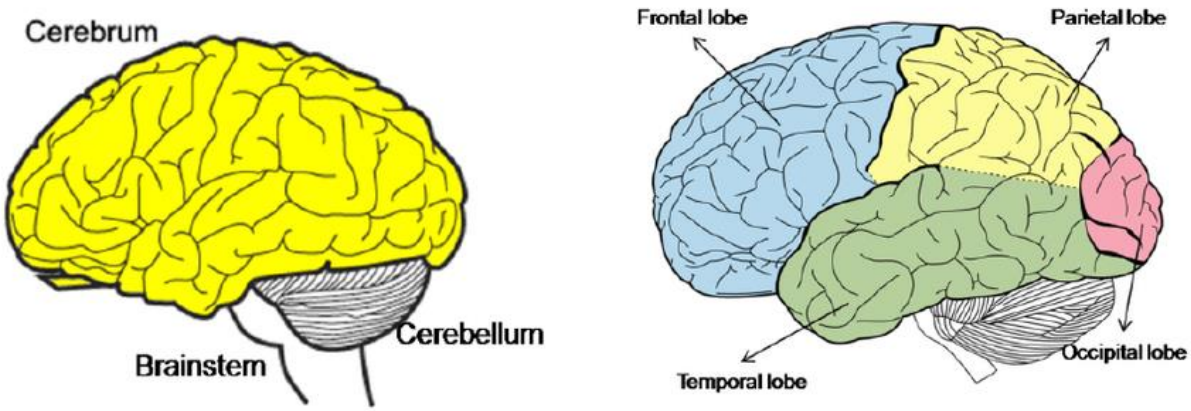

Figure 2. Illustration of the main anatomical brain regions. (Taken from Widmaier et al., 2004)

Lastly, the cerebrum is the largest part of the brain and is divided into two hemispheres. Each hemisphere is further divided into four lobes: frontal, parietal, temporal, and occipital (Fig. 2 Right). The cerebrum is responsible for higher brain functions, including cognition, emotion,

memory, and sensory processing. The frontal lobe is associated with reasoning, planning, parts of speech, movement, and problem-solving. The parietal lobe processes sensory information related to touch, pressure, temperature, and pain. The temporal lobe is involved in perception and recognition of auditory stimuli, memory, and speech, while the occipital lobe is primarily responsible for visual processing. Together, these regions of the cerebrum enable complex behaviors and the ability to interact with and interpret the world around us (Kolb & Whishaw, 2015).

The frontal lobe is further separated into four main areas: the prefrontal, the premotor and the motor cortex, and Broca's area. The prefrontal cortex is involved in complex cognitive behavior, decision-making, personality expression, and moderating social behavior, playing a crucial role in executive functions such as planning, problem-solving, and impulse control (Fuster, 2014). The premotor cortex is responsible for the planning and coordination of movement, preparing the body's muscles for the exact movements that will be carried out by the motor cortex (Wong et al., 2015). The motor cortex, located just anterior to the central sulcus, is directly involved in the execution of voluntary movements by sending signals to the muscles, allowing for precise and coordinated physical actions. Broca's area, typically located in the left hemisphere, is essential for speech production and language processing, enabling the articulation of thoughts into spoken words (Kandel et al., 2013).

The CNS is composed of two main cell types: neurons and glial cells. Neurons are the primary cells responsible for transmitting and storing information within the brain, communicating through electrical impulses. These impulses are crucial for all brain functions and can be measured using techniques such as EEG, which will be explored in detail in the next section. The CNS contains approximately 86 billion neurons, with the majority (~69 billion) located in the cerebellum and about 16 billion in the cerebral cortex(Azevedo et al., 2009). Each neuron forms synaptic connections with roughly 10,000 others, creating a vast network that underlies the complex processing abilities of the brain.

2.2. Electroencephalography

2.2.1. Biophysics of neural signals

To understand the biophysics behind the measured electrical signal, we can decompose neural activity into three spatial scales: the microscopic single neuron scale (nm-um), populations of

neurons at the mesoscopic scale (um-mm) and major brain regions at the macroscopic scale (mm-cm) (Fig. 3).

At the smallest scale, we have what is considered the unit of the CNS, the neuron. Despite having different morphologies and electrophysiological properties, typical neurons consist of four principal components: the cell body or soma, one axon, dendrites and presynaptic terminals. The dendrites receive incoming electrical signals from other neurons and pass them along to the soma, which houses the nucleus and organelles. If the sum of these signals surpasses a given threshold, the neuron fires, i.e., a signal is transmitted through the axon onto other neurons via the presynaptic terminals (Bigbee, 2023).

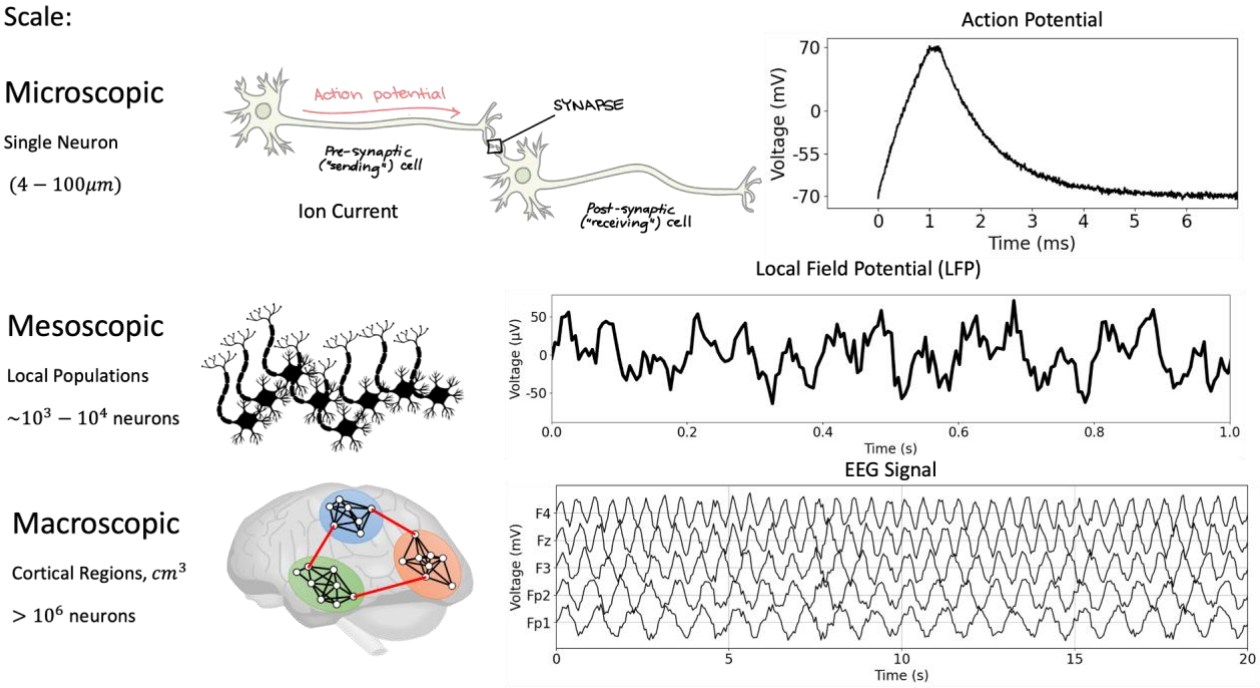

Figure 3. The different scales of neuronal electrical signaling. Schematic of the three different scales of the biophysics of neural signals.

At this level, the electrical signal carried through a single neuron is called an action potential (also referred to as spike), and it occurs through the quick rise and fall of the membrane potential along the neuronal cell (Hodgkin & Huxley, 1952). These changes are generated by voltage-gated ion channels at the cell membrane and are most commonly initiated by excitatory postsynaptic potentials from a presynaptic neuron. These channels consist of proteins whose configuration switches as a function of the voltage between the interior and exterior of the cell, i.e., the membrane potential. This electric potential is caused by an electrochemical ion gradient actively maintained by ion pumps at the membrane. In turn, this ion gradient results from a high extracellular concentration of sodium (Na+) and chloride (Cl-) ions and a high

intracellular concentration of potassium (K+) ions, generating a negative resting membrane potential (around -70mV). The voltage-gated ion channels remain closed at the resting membrane potential, and rapidly open whenever the membrane potential reaches a certain threshold (around -55mV), causing a sudden influx of sodium ions, producing an even greater rise in the membrane potential (see Fig. 3). At around 40mV, membrane repolarization occurs from rapid sodium channel inactivation as well as activation of potassium channels, causing an efflux of potassium ions, setting the membrane potential back to resting state after a brief hyperpolarization period. This event causes neighboring voltage-gated channels to open, producing an ionic current that changes the extracellular potential in a domino-like propagation, carrying the signal along the neuron and onto other neuronal cells (Hammond, 2015). A single-unit recording using a microelectrode system provides a method of measuring a single spike. This system usually consists of a glass micropipette with a metallic microelectrode placed close to the cell membrane, allowing the ability to record the extracellular field (Humphrey & Schmidt, n.d.).

At the mesoscopic scale, electrical activity of individual cells within a larger population of neurons (~10^4 neurons) generates what is called a local field potential (LFP) in that tissue. The LFP represents the summation of the extracellular electrical fields generated by single spikes and is recorded using intracranial microelectrodes placed sufficiently far from individual neurons to avoid any single cell dominating the measurement. A low-pass filter (~300Hz) is then applied to remove any spike component of the signal, resulting in the lower frequency LFP signal (Buzsáki et al., 2012).

Finally, at the macroscopic level, several populations of neurons generate an electric signal that reflects the averaged summation of the synchronous activity of hundreds of millions of neurons with a similar spatial orientation, creating voltage field gradients that can be detected at the surface of the cortex (electrocorticography) or even from outside of the skull at the scalp (EEG) (Buzsáki et al., 2012). Action potentials are too short to sufficiently sum up to be recorded extracellularly by electrodes on the scalp. However, postsynaptic potentials of cortical pyramidal cells can last up to 10ms and are able to produce sufficient potential changes to be measured by EEG. Postsynaptic potentials are caused by presynaptic potentials releasing neurotransmitters into the synaptic cleft and binding to postsynaptic receptors. Most of these receptors consist of ion channels that change conformation as they bind to a neurotransmitter, causing an influx/efflux of ions and changing the membrane potential. At excitatory synapses, the ion channels allow sodium into the cell, generating a depolarizing current that causes an

increase in membrane potential, known as an excitatory postsynaptic potential (EPSP). This increased potential at the postsynaptic membrane is measured as a negative voltage in the extracellular space due to the preponderance of negatively charged ions. In contrast, at inhibitory synapses, ion channels allow for a potassium outward current, hyperpolarizing the cell and producing a stronger negative membrane potential, known as an inhibitory postsynaptic potential (IPSP). Analogous to the EPSP, the IPSP is measured extracellularly as a positive voltage due to the preponderance of positively charged ions (Kirschstein & Köhling, 2009).

Given their unique anatomical structure with a long apical dendrite perpendicular to the cortical surface (i.e., neurons located in the gyri), cortical pyramidal neurons work as excellent dipoles for electrical signal generation (Fig. 4). Pyramidal cells are highly polarized and the main excitatory neurons in the cerebral cortex responsible for generating the EEG signal. The direction of the dipole and the deflection in the measured signal is determined by the superficial or deep location and polarity of the synaptic input. By convention, a positive scalp potential is recorded as a downward deflection in the EEG signal. Thus, superficial excitatory inputs and deep inhibitory inputs are measured as upward deflections, whereas deep excitatory and superficial inhibitory inputs are registered as downward deflections (Kirschstein & Köhling, 2009; Nunez & Srinivasan, 2009).

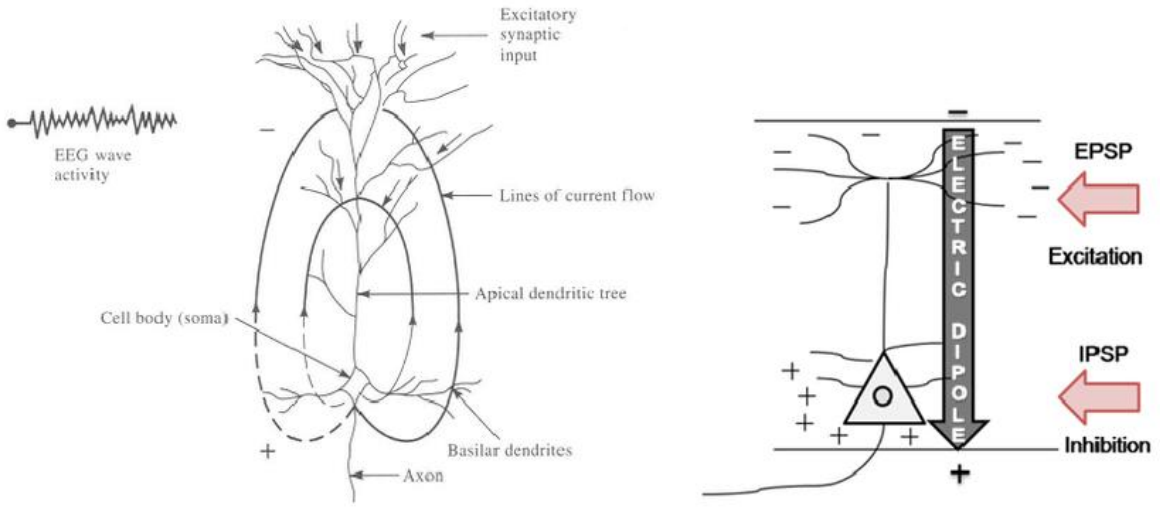

Figure 4. Pyramidal cell as an electric dipole. Negative polarity in the extracellular space is caused by an influx of positive charge carriers, an excitatory synaptic input (EPSP). These positive charges then spread along the apical dendrite, and through capacitive efflux, they generate an extracellular positive potential at a distance from the synapse, such as at the soma.

This produces a dipole with sufficient strength to be measured by the electrode on the scalp (Adapted from Kirschstein & Köhling, 2009; Neuman, 1998).

2.2.2. Frequency Bands

To yield a visible EEG signal, a sufficiently large number of simultaneous and in the same direction EPSPs and IPSPs are needed. The amplitude and frequency of the recorded EEG wave is determined by the firing rate and synchronicity of postsynaptic potentials evoked by a population of pyramidal cells. The more synchronous a population of neurons fires at a given rate, larger the amplitude of the summed EEG gets at that given frequency (Kirschstein & Köhling, 2009). As the neurons desynchronize, the amplitude decreases and the frequency increases (Fig. 5). If all neurons in a population were active synchronously, the frequency of the measured EEG wave would be identical to their firing rate. The extent to which neurons synchronize at specific frequency bands depends on the current level of vigilance. The highest levels of synchronization occur during deep sleep, resulting in measured theta (4-7 Hz) and delta (0.5-4 Hz) waves (Ferrillo et al., 2000; Moroni et al., 2012). During awake resting, when sensory inputs are reduced, we obtain moderately synchronized EEG alpha waves (8-13 Hz) (Darracq et al., 2018; Foxe & Snyder, 2011). When actively engaged in a cognitive or motor task, with open eyes and at the presence of sensory inputs, the neuronal activity desynchronizes, producing non-synchronous EEG beta waves (13-30 Hz) (Avanzini et al., 2012). It is important to note that there are slight variations in the literature regarding the exact ranges of these frequency bands, but we have chosen to use the most widely accepted ranges for consistency. All the frequency bands, their usual location and main functions are detailed in Table 1.

Table 1. EEG frequency bands details.

Frequency Band (Hz)	Location	Function	Visualization
Delta (<4)	Frontal (adults) Posterior (children)	Slow-wave sleep	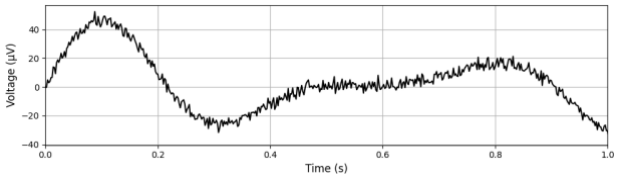
Theta (4-7)	Found in location unrelated to task at hand	Associated with inhibition of elicited response. (Kirmizi-Alsan et al., 2006)	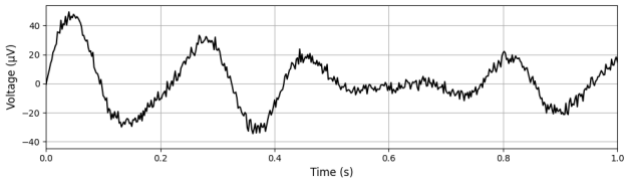
Alpha (8-13)	Central & Occipital at rest. Lower in locations related to task.	Relaxed/at rest Associated with inhibitory control.	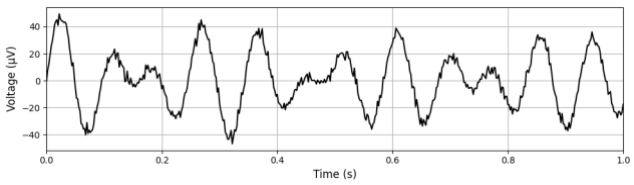
Beta (13-30)	Most evident frontally.	Active thinking, focused, high alertness.	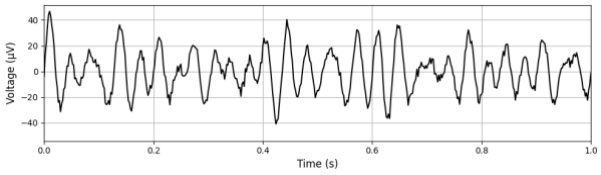
Gamma (>32)	Somatosensory cortex.	Cross modal sensory processing. (Kisley & Cornwell, 2006) Short-term memory matching	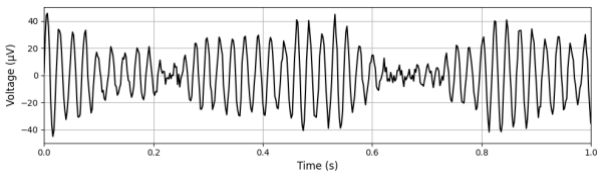

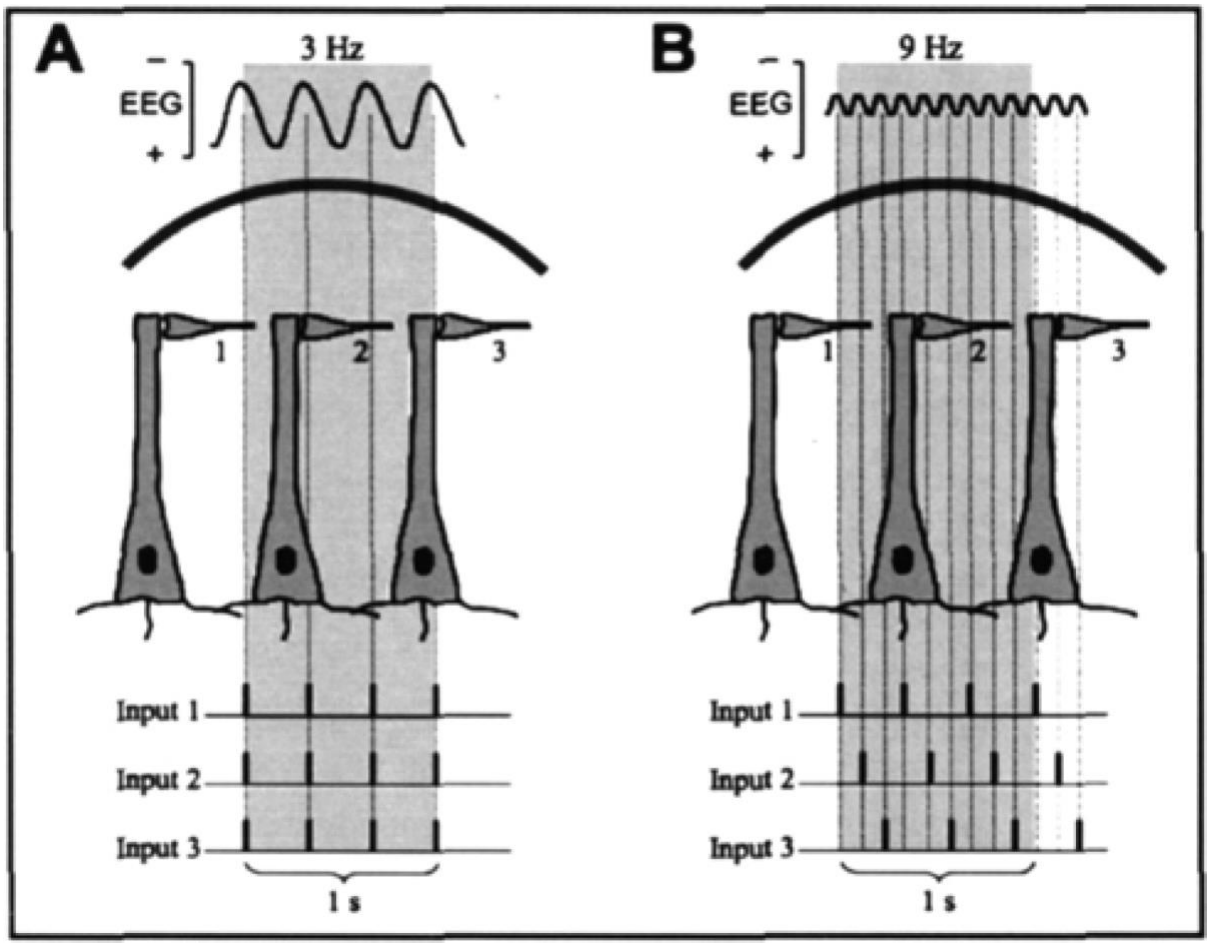

Figure 5. Synchronization and desynchronization are illustrated for three pyramidal neurons, each receiving a superficial excitatory input (EPSP) at a rate of 3Hz. In the synchronized EEG (A), all three inputs fire simultaneously, allowing the EPSPs to sum and produce a 3 Hz EEG wave at the scalp. In contrast, a desynchronized EEG (B) with lower amplitude and higher frequency occurs when the three inputs fire alternately. In this case, the EEG amplitude does not sum, but its frequency increases to 9 Hz. (Adapted from Kirschstein & Köhling, 2009)

2.2.3. EEG Equipment

EEG Electrodes

EEG electrodes are one of the very basic elements in the process of measuring electrical activity in the brain. They are the real contact medium between a subject's scalp and an EEG system and detect the electrical potential produced by populations of neurons. This is a non-invasive process, during which the electrodes can pick up minute signals with low amplitude, prone to attenuation. Therefore, the precision of signal acquisition and the quality of data obtained are heavily influenced by the choice of electrodes (Angrisani et al., 2017; Yuan et al., 2021).

There are different shapes of EEG electrodes: disc, needle, and cup shape; and dry or gel-based can be another classification. A direct contact exists between the electrode and the scalp with dry electrodes (Yang et al., 2022), whereas a conductive gel is used with gel-based electrodes to better conduct the signals, in an attempt to reduce impedance at the electrode-skin interface.

Commonly, electrodes are made from a conductive metal that supports the exchange of ions and electrons at the surface that has direct contact with electrolytes (in the case of gel systems). This interaction is critical for the detection of signals, but it can introduce complexities such as the half-cell potential, which arises from the differing rates of ion and electron layer formation (Usakli, 2010) This potential can affect signal quality, making it essential to consider electrode material when setting up an EEG system.

A major distinction in the operation of electrodes is whether they are polarizable or nonpolarizable. Nonpolarizable, or reversible electrodes, such as Ag-AgCl electrodes (Fig. 6A), allow a free exchange of charge across the electrode-electrolyte interface, minimizing impedance and reducing artifacts caused by motion. These electrodes, consequently, are widely used because they can adequately record slow potential changes with minimal signal interference (Beltramini, 2014; Picton et al., 2000). Polarizable (nonreversible) electrodes have a restricted charge exchange across their double layer, effectively acting as capacitors. While these electrodes can filter out high frequencies and DC voltages, they are less commonly used in standard EEG setups due to their potential to distort the recorded signal (Usakli, 2010)

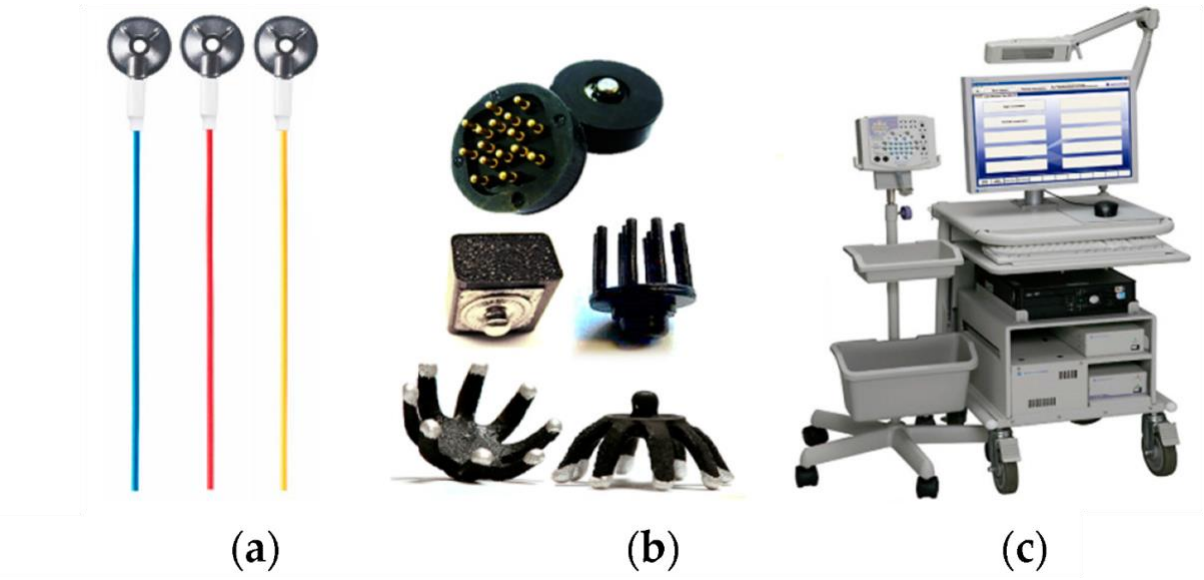

Figure 6. Illustration showing different components from the EEG equipment. (a) standard Ag/AgCl wet electrodes; (b) variety of dry electrodes; (c) EEG monitoring system. (Adapted from O'Sullivan et al., 2019)

The impedance at the electrode-tissue interface is of great importance in EEG recordings and determines the quality of the signal and the signal-to-noise ratio. High impedance can lead to poor signal quality, and several factors can contribute to it, such as lack of skin preparation, hair presence, and electrolyte conditions. The skin should be prepared by cleaning the skin of oils and dirt, and if gel electrodes are used, the gel must fill the space between the electrode and the scalp. Poor contact, or inadequate gel, introduces noise and artifacts into the data (Fortune et al., 2021).

The choice between dry and gel electrodes depends on the specifics of the application at hand and experimental requirements. Gel electrodes are known for providing more consistency, which refers most importantly to those setups where low impedance and high signal quality are important (Vojkan Mihahlovic & Garcia-Molina Gary, 2012). However, dry electrodes are easier to manipulate and can be used in a series of applications for which expedient setups and ease of use are the most important (Lopez-Gordo et al., 2014).

Amplifier

EEG amplifiers are essential in the recording process as they amplify the low amplitude electrical signals generated by brain activity. These signals are typically in the microvolt range,

making them prone to interference from environmental noise. The EEG amplifier is a differential amplifier, designed to amplify the difference between two input signals while suppressing any voltage that is common to both (Laplante, 2005). This is particularly beneficial in EEG recordings, as it helps eliminate environmental noise, such as electromagnetic interference, which can be much stronger than the brain signals themselves.

The signals processed by the amplifier depend on two key points: the ground electrode and the reference electrode. The ground electrode is the one designated to be at zero potential, serving as the electrical baseline. The reference electrode is ideally placed on an electrically neutral part of the body, although this is hardly ever achievable. In practice, the EEG signal recorded at each electrode is relative to the potential at the reference electrode (Beltramini, 2014). Common sites for placing reference electrodes include the mastoids, ear lobes, or nose (Kulaichev, 2016). Additionally, in larger EEG setups, it is possible to use the average signal from all electrodes as a reference, which can provide more balanced and accurate readings across the scalp (Rosenfeld, 2000).

One of the amplifier's most critical features is its common mode rejection (CMR) capability, which refers to the ability of the amplifier to reject common signals between the two inputs (Kappenman & Luck, 2010). The higher the CMR, the better the signal-to-noise ratio (SNR), meaning that more brain signal and less noise will be recorded. For effective CMR, the impedance of the electrodes relative to the amplifier’s input must be optimized. Poor electrode impedance can result in a decreased CMR, leading to a lower SNR.

The impedance of the electrodes is largely influenced by skin properties, and higher electrode impedance can reduce the effectiveness of CMR. In high-impedance systems, more trials may be necessary to average out noise and improve SNR, which can make the recording process longer and more complex. This is why low-impedance electrodes are often preferred, as they typically result in cleaner recordings with better statistical significance (Habibzadeh Tonekabony Shad et al., 2020).

To minimize impedance, abrasive creams are often used to remove the outer layers of the skin and improve contact between the electrode and the scalp. However, this process can be time-consuming and uncomfortable for the subject, and in some cases, skin abrasion can cause bleeding, which requires additional electrode cleaning and disinfection (Khoa et al., 2013).

An alternative to using low-impedance electrodes is to use high input impedance amplifiers, which can work effectively with high-impedance electrode systems (Kappenman & Luck,

2010). These amplifiers can handle the reduced SNR that comes with high-impedance electrodes, although they do not solve all issues. One persistent problem with high-impedance systems is the presence of skin potential artifacts, which arise from differences in the conductance of the skin beneath the electrodes. These artifacts can introduce unwanted electrical potentials, which fluctuate over time. To minimize skin potential artifacts, it is important to maintain a cool and dry recording environment to reduce sweating, as changes in sweat levels can affect the skin's electrical properties (Kappenman and Luck 2010).

Electrodes Positioning System

The electrode positioning systems of 10-20 and 10-10 represent two standardized approaches in EEG recordings to get accurate and consistent placement of electrodes on the scalp. Both were developed as guidelines that offered a more uniform system so that results obtained between different studies and participants could be compared with validity (Jurcak et al., 2007).

The numbers "10" and "20" refer to the percentage distances between adjacent electrodes - taken from the total circumference of the head. In the 10-20 system, electrodes are placed at an interval of either 10% or 20% from this distance, providing balanced coverage of the scalp with a reasonable number of electrodes (Fig. 7 Left). This system is widely used for clinical EEG recordings with 21 electrodes. The 10-10 system is an extension of the 10-20 system because it inserts electrodes at 10% intervals, resulting in a much higher electrode density amounting to 64 or more electrodes (Fig. 7 Right) (Oostenveld & Praamstra, 2001). This is considered to be especially useful for research studies where finer spatial resolution is required. In both systems, electrode positions are named using a combination of letters and numbers.

Letters identify the scalp region underneath which the electrode is positioned: F for frontal, T for temporal, P for parietal, O for occipital, C for central. Numbers refer to the relative position: odd numbers are on the left hemisphere, even numbers are on the right hemisphere, "z" indicates electrodes along the midline. This standardized system allows for the precise and repeatable positioning of electrodes, which is very important in ensuring recordings of brain activity come from the same regions in subsequent sessions or different subjects. Although the 10-10 system is more appropriate for research where detailed spatial mapping of brain activity is a critical factor, the 10-20 system can normally suffice in routine clinical use (Jurcak et al., 2007).

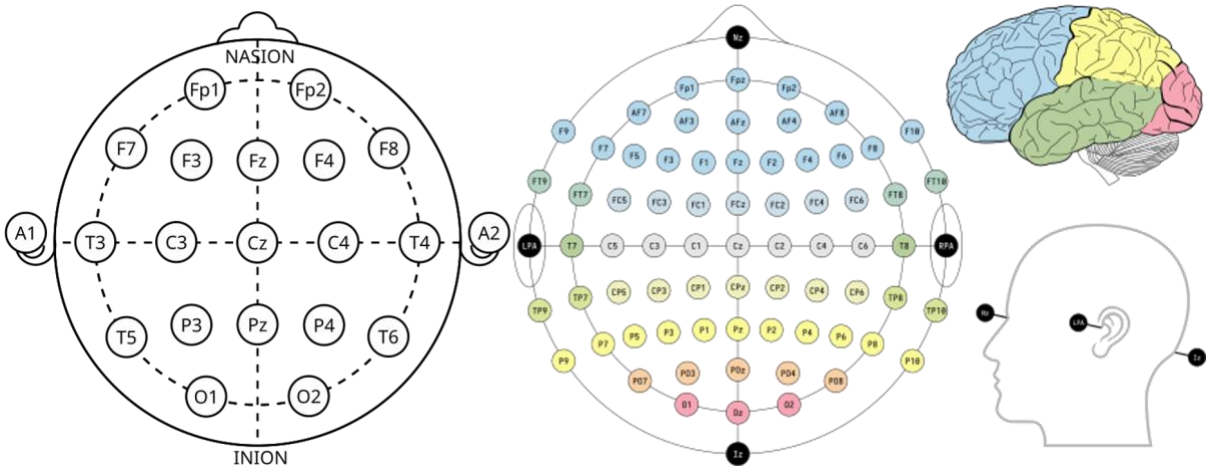

Figure 7. EEG Positioning Systems. Left: 10-20 positioning system. Right: 10-10 positioning system with colors representing the different major brain regions.

2.2.4. Signal Artifacts

EEG is known to produce a relatively noisy signal due to the distance between the sensors and the brain's signal source and the various contaminants that can affect its quality. Artifacts—any measured signals that do not originate from the brain—are common in EEG recordings. These artifacts can be physiological, such as those caused by eye blinks, cardiac activity, or muscle movements; they can also stem from instrumentation issues like faulty electrodes, line noise, or high electrode impedance; or they can be environmental, such as head or limb movements. These artifacts can introduce bias into analyses or compromise the overall quality of the signal, making their identification and removal crucial for accurate EEG interpretation (Jiang et al., 2019).

Physiological artifacts

Eye movements and blinks can propagate across the scalp and be detected as part of the EEG signal, causing ocular artifacts, which represent a significant source of interference in EEG recordings (Wallstrom et al., 2004). Specifically, eye movement artifacts are generated by changes in the orientation of the retina and cornea dipole, while blink artifacts result from variations in ocular conductance due to the cornea's contact with the eyelid. Due to the volume conduction effect, both ocular artifacts and EEG activity spread to the surface of the head and are recorded by the electrodes. These ocular signals can be measured using electrooculography (EOG), which typically has a much greater amplitude than EEG signals and shares a similar frequency range (Fig. 8) (Wallstrom et al., 2004). It is important to note that EEG data can be

contaminated by EOG signals, and conversely, EOG signals can also be affected by EEG activity.

Muscle artifacts, also known as electromyography (EMG) artifacts (Fig. 8), are a significant challenge in EEG data analysis due to their origin from various muscle groups and their wide frequency distribution (Goncharova et al., 2003). These artifacts are caused by muscle activity near the EEG recording sites, such as when a subject talks, swallows, or moves, making them particularly problematic in uncontrolled environments (Urigüen & Garcia-Zapirain, 2015). Unlike ocular artifacts, EMG contamination is more difficult to eliminate because it arises from the electrical activity generated by contracting muscles across the head, face, and neck, leading to a broad spectral distribution that can overlap with all classic EEG frequency bands. For instance, EMG activity often overlaps with the beta (15–30 Hz) and alpha (8–13 Hz) bands, but can also be as low as 2 Hz, making EEG signals especially vulnerable to interference (Urigüen & Garcia-Zapirain, 2015).

The amplitude and waveform of EMG artifacts vary depending on the degree of muscle contraction and the type of muscle involved, making these artifacts difficult to characterize and stereotype. Additionally, EMG signals can be detected across the entire scalp due to volume conduction, and they exhibit substantial statistical independence from EEG activity both temporally and spatially. This independence suggests that techniques like Independent Component Analysis (ICA) may be suitable for removing EMG contamination (Chen et al., 2016). However, EMG artifacts are particularly challenging to correct because they are temporally mixed with various experimental conditions, such as cognitive load and vocalization, and lack the repetitive patterns seen in other biological artifacts. This complexity underscores the difficulty in effectively isolating and removing EMG artifacts from EEG recordings.

Cardiac artifacts in EEG recordings arise primarily from the electrical activity of the heart, measured by the electrocardiogram (ECG) (Fig. 8), and from pulse artifacts when an electrode is placed over or near a blood vessel. ECG artifacts typically have a low amplitude on the scalp, but this can vary depending on electrode placement and individual body types. The ECG has a distinct, repetitive pattern, which can sometimes be mistaken for epileptiform activity, especially when it is faintly visible in the EEG. Despite this, ECG artifacts are relatively easy to correct since they are routinely recorded alongside cerebral activity, providing a reference waveform for artifact removal (Lee et al., 2015).

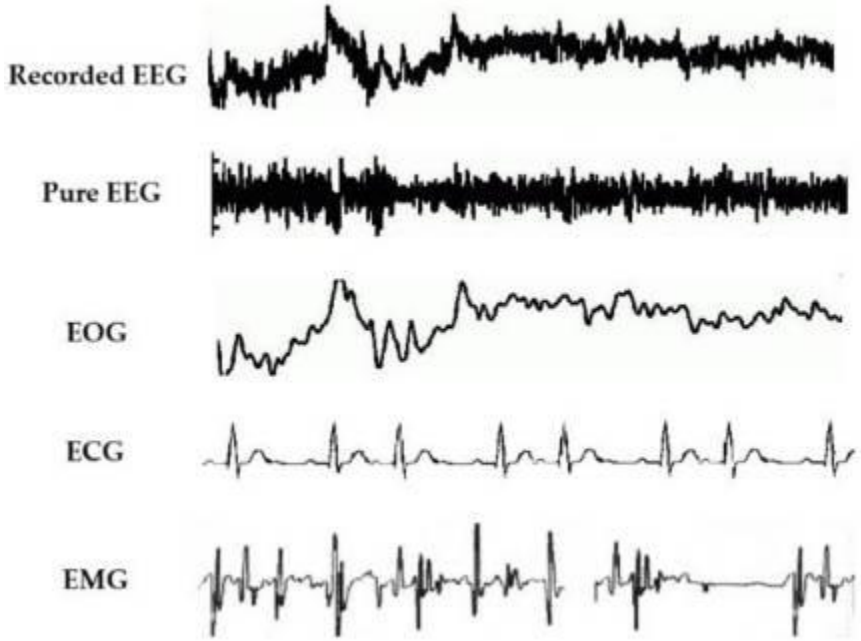

Figure 8. Physiological artifacts on EEG signal. (Taken Jiang et al., 2019)

In contrast, pulse artifacts are more challenging to address. These occur when an EEG electrode is positioned over a pulsating vessel, such as a scalp artery, leading to slow periodic waves that can resemble actual EEG signals (Hamal & Rehman, 2013). The frequency of pulse artifacts is typically around 1.2 Hz, making them difficult to differentiate from EEG activity due to their similar waveform. However, pulse artifacts generally affect only one electrode and can be minimized by careful sensor positioning. A direct relationship exists between ECG and pulse activity, with pulse waves occurring at regular intervals preceding the ECG. While ECG artifacts can be mitigated using a reference waveform, pulse artifacts are more stubborn due to their similarity in time and frequency to the underlying EEG signal (Hamal & Rehman, 2013).

Non-physiological artifacts

The measured EEG signal is also contaminated by various non-physiological artifacts, caused by external environmental factors unrelated to the body's physiological processes. A common

cause of these artifacts is movement in electrodes, whereby even the slightest of movements may cause spurious signal spiking. Likewise, an imbalance in electrode impedance — often due to insufficient contact between electrodes and the scalp — can introduce errors into recordings by boosting noise or attenuating actual EEG signals. Another common non-physiological artifact is caused by powerline interference, often around 50 or 60 Hz due to electromagnetic fields from other electrical devices in the environment. Furthermore, any movement in the head body or limbs while recording EEG can lead to an artifact as this may shift electrodes or induce muscle noise that would interfere with signals obtained. Of all the types of artifacts, non-physiological artifacts are particularly difficult to control as they frequently share a frequency range with actual EEG activity which can only be minimized through attention toward electrode placement, impedance balancing and minimization of environmental noise (Kaya, 2022).

2.2.5. Preprocessing

An EEG data preprocessing pipeline specifies a step-by-step procedure of remodeling the raw EEG data into a cleaner signal by removing unwanted artifacts and noise, thereby converting the measured signal into a more suitable format for analysis and interpretation (Fig. 9). Several preprocessing techniques have been developed and described within the published literature; for this work, we chose the Harvard Automated Processing Pipeline for Electroencephalography (HAPPE), a state-of-the-art standardized and automated preprocessing software (Lopez et al., 2022). We specifically used HAPPE in Low Electrode EEG (HAPPILEE) for lower density recordings (<32 channels). The main steps in the pipeline are described in detail below and can be seen in the schematics (Fig. 9).

Line noise processing

HAPPILEE successfully mitigates electrical noise at 60 or 50 Hz by multiple tapers regression that is based on the CleanLineNoise program (Tim Mullen, 2012). This technique is capable of detecting and removing common sinusoidal signals at particular frequencies (e.g., electrical noise), without overly affecting or corrupting the source EEG signal within those and nearby frequency bands—a phenomenon commonly observed with traditional notch filtering techniques for line-noise processing. The multi-taper regression (CleanLineNoise) searches for line-noise signals around the user-specified frequency ± 2Hz, using a combination of

approaches. This control method is capable of narrowing in with a high degree of precision on the electrical noise frequency (setpoints are selectable at 60 Hz and 50 Hz). For similar cleaning, users may also define harmonic frequencies (e.g., 30 Hz & 15 Hz) or close frequencies using a nearby frequency pair (e.g., use both pairs: 59 Hz and 61 Hz for a specific location like a 60 Hz signal). HAPPILEE calculates the quality control metrics for regular sinusoidal signal removal at these frequencies and automates their output as a quality assessment report.

Band-pass filtering

Filtering of the EEG signal is necessary in order to isolate relevant frequencies and improve the signal-to-noise ratio (i.e., for ERP analyses or isolating frequencies generated by different sources), but it can also help filter unwanted frequencies. However, if not undertaken carefully, setting the filtering options can distort your data in a harmful way (see Tanner et al., 2015; Widmann et al., 2015) for why some EEG filters are problematic) both by themselves and in combination with other processing steps.

HAPPILEE uses the pop_eegfiltnew function in EEGLab, which applies a zero-phase Hamming-windowed sinc FIR filter, for preliminary filtering before channel rejection (if selected by the user) and applying artifact correction methods across all files. During preprocessing of resting-state EEG or task-based data for time-frequency analyses, this entails applying a band-pass filter ranging from 1 to 100 Hz. The higher cutoff for the low-pass filter at 100 Hz allows better detection of bad channels, and improves artifact correction, especially for EMG and other high-frequency artifacts that can contaminate the data.

Bad channel detection

HAPPILEE also provides a way to detect channels that contain no usable brain data (e.g., due to high impedance, broken electrodes/connections, poor scalp contact, excessive movement, or muscle-related artifacts like EMG noise). Users can choose to initiate the bad channel detection or skip it; however, it does run through the subsequent processing steps with all channels. In the chosen automated pipeline, different steps were employed to detect and remove bad channels, but some common techniques should be modified because they were designed for high-density EEG (especially those based on standard deviations), so these methods may not work well in low-density EEG.

Artifact correction

The raw EEG data quality usually suffers from various artifacts (e.g., motion, electromyogenic activity, or eye movement/blink) that need to be tackled during preprocessing steps. Historically, artifact-laden timestamps were generally recognized by visual inspection of the data and executing a removal of epochs for affected electrodes, an approach referred to as artifact rejection. HAPPILEE instead uses wavelet thresholding methods for artifact correction, without the removal of any timepoints. This artifact correction is performed on every electrode individually, and is therefore applicable for any channel density, from single-electrode recordings upwards. Since the performance of wavelet thresholding does not depend on channel density, it can always be expected to work reasonably well (i.e., to capture meaningful patterning) irrespective of whether high- or low-density setups are used. This property also pushes wavelet-thresholding to an optimal selection for many low-density EEG setups.

Wavelet-thresholding consists of three main steps (Lopez et al., 2022):

Step 1: Apply the wavelet transform. The EEG data is subjected to the wavelet transform, which consists of fitting a wavelet function to represent signals over time and dividing them into various frequency regions (similarly to bandwidths). Wavelet functions provide a class of orthogonal bases, which are compressed in various forms (families) and applied to different signal compression, denoising, or representation tasks. These wavelet functions resemble the oscillatory shape of EEG data. Not only that, but the temporal resolution of these wavelet functions is also very good, which means that they can represent information in time and frequency accurately. The process carries the selected wavelet function over all time points, producing a set of coefficients describing how well this signal fits at every point in the timeseries. It is important because good fitting for EEG signals depends on the function selection, affecting artifact-correction integrity. The transform also decomposes the EEG signal into several frequency bands, and coefficients quantify variations of the signal within each frequency band separately. As a result, the wavelet transform works similarly to a frequency filter, which is subsequently reversed and does not leave any footprint in the remaining EEG data. Each wavelet function comes with a resolution level, or level of decomposition, that dictates the number of these frequency bands into which the EEG signal will be separated (higher levels parse out lower frequencies into finer and finer bins). When the resolution level is not determined appropriately, useful low-frequency information can be lost during thresholding.

Step 2: Threshold the data to isolate artifact signals. Wavelet transform coefficients that describe the EEG within each frequency bin are then thresholded to remove artifact signals from neural signals. This is precisely the aspect that allows for artifact detection at specific frequency bands relative to neural data within those same frequencies—a foundational property of the wavelet-thresholding's success with EEG signals. Since the artifact signal is of a greater magnitude than the neural signal at similar frequencies and occurs less predictably among the fluctuations in this frequency range due to brain-related activity, wavelet coefficients displaying these features are identified as being from an artifact-signal component, which will then be subtracted directly from the data through thresholding. However, if the resolution level of a wavelet is set too low, band-passed neural data—specifically with lower frequency and presumably higher electrical amplitude than other frequencies in EEG signals—is erroneously classified as an artifact.

The threshold can be determined and applied to all frequency ranges (level-independent threshold) or adapted independently per frequency band based on the signal characteristics at that specific range (frequency-dependent thresholds). This level-dependent threshold is utilized by HAPPILEE to fit the properties of artifacts unique to each frequency spectrum. After applying the threshold to identify which wavelet coefficients (representing pieces of the EEG signal) are above the threshold, they can be subtracted as artifact-related signals. Additionally, the treatment of these thresholded coefficients can be resolved in multiple ways known as "threshold rules." HAPPILEE employs a hard threshold (i.e., the sub-threshold coefficient is entirely removed from the data) to uniquely separate artifact-related signals. Other rules, such as the soft threshold, instead downweight these sub-threshold coefficients closest to the optimal value in the data. If these steps collectively are not optimized for EEG signals, this can lead to either incomplete artifact correction or attrition of the neural signal altogether. After successfully separating the artifact signal from the neural signal, this information can be removed by performing an inverse wavelet transform and subtraction without influencing the timepoints where dominant underlying neural signals are present.

Step 3: Inverse wavelet transform and subtraction of thresholded (artifact) signal. Finally, artifact-related coefficients can be transformed back to the signal time series using the inverse function of the wavelet transforms. The HAPPILEE wavelet function set accomplishes this without damaging data in any space: phase, amplitude, or frequency. This inverse transform produces an artifact time series, which is then subtracted from the electrode's original time series, resulting in the artifact-corrected signal. Since waveleting is a method that is time- and

frequency-specific, the artifact time series will be mostly zeros where no artifactual pattern appears in a temporal region of data, ensuring that this subtraction doesn't disturb any brain signal not contaminated by the artifact. This aspect distinguishes wavelet-thresholding from other methods like ICA, which do not consistently maintain such constraints and may introduce distortions in signals outside the artifact period. The wavelet-thresholded artifact-corrected signal may then proceed to further pre-processing steps like re-referencing.

Re-Referencing

Although there is no perfect reference for EEG, re-referencing using various pragmatic though imperfect options can cancel out artifact signals shared across electrodes (e.g., residual line-noise) while recovering signals from online reference channels of interest. If re-referencing, the user can either average-reference across channels, reference to one or multiple other electrodes' subset of channels or use the reference electrode standardization technique (REST) at infinity (for more on REST, see Yao, 2001). This highlights the importance of a reflective decision between re-referencing methods per dataset, particularly when using a low-density montage (e.g., Junghöfer et al., 1999). Users may re-process data with different options to assess how a re-referencing scheme affects their results.

One major concern with low-density layouts is inter-electrode distance. Since the number of channels is limited, re-referencing to one or a subset of channels may lead to biases if the electrodes are far apart on the scalp If the reference electrode is close to some electrodes but far from others, it may only reflect an artifact of electrical activity obtained at a macro level (Lei and Liao 2017). If the user decides to re-reference to a channel subset, they must ensure that these channels' amplitudes are comparable in magnitude with signals from other electrode sites and that they are not involved in task-induced activity (Kim, 2018).

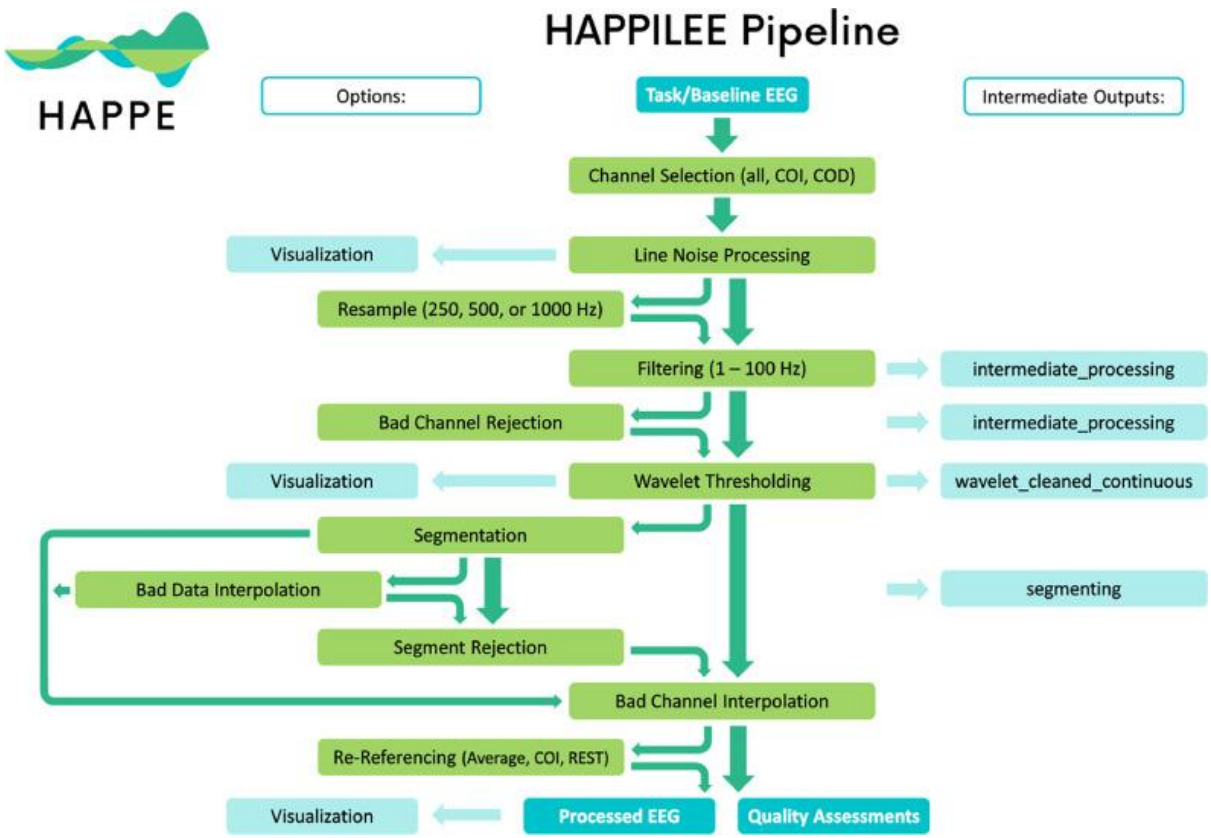

Figure 9. Schematic diagram of the HAPPILEE pipeline's pre-processing steps. (Taken from Lopez et al., 2022**)**

2.3. Method of Analysis

In order to extract meaningful information about the underlying brain dynamics from EEG data, several quantitative methods of analysis have been developed throughout the years. In this work, we performed a connectivity analysis, which calculates statistical dependence and information flow between cortical regions (i.e. EEG channels). This technique was implemented via the use of several Python libraries (MNE) and MATLAB based software such as EEGLab (Delorme, 2004) and Brainstorm (Tadel et al., 2011) and are further detailed below.

2.3.1. Connectivity Analysis

There has been a growing interest in studying brain function not only by identifying variations in activation of brain areas but also by mapping the interactions among the neural assemblies distributed across brain regions. This concept is addressed in neuroscience as the functional integration principle, i.e. the coordinated activation of neural populations distributed across different cortical areas that constitute brain-wide distributed functional networks. Integration of cerebral areas can be measured by estimating brain connectivity in two different ways: structural or functional connectivity.

Structural connectivity is defined as the degree to which regions are anatomically connected by fiber pathways that track over extended regions of the brain (Park & Friston, 2013). Anatomical connectivity is usually estimated using a combination of imaging modalities such as magnetic resonance imaging (MRI) and diffusion tensor imaging (DTI) and mathematical modeling to map the white matter fiber tracts that connect distant brain structures (Gong et al., 2009). Neuroanatomical connectivity was not an object of study in this work, but it represents an important component of several other connectivity analyses as it establishes the anatomical structure underlying most functional networks.

Functional connectivity is defined as the temporal correlation of neurophysiological events occurring in anatomically separated brain regions (Fingelkurts et al., 2005). A variety of neurophysiological signals can be studied through the lens of functional connectivity, including signals originated from LFP measurements, EEG, magnetoencephalography (MEG), positron emission tomography (PET), fMRI and functional near infrared spectroscopy (fNRIS). Various mathematical methods exist to estimate the temporal correlation between pairs of signals, with each method being more appropriate for specific signal types and the particular objectives of

the analysis. In this work, we chose phase lag synchronization as the main technique to estimate functional connectivity.

Phase Synchronization

The concept of phase synchronization comes from the description of chaotic oscillators in the synchronous regime where the phases are locked or simply bounded by a constant value (Rosenblum et al., 1996). Defining ϕ_1 and ϕ_2 as the phases of two time series x_1 and x_2, and $\Delta\phi$ the phase difference between them (Fig. 10), the phase synchronization holds as long as:

$$\Delta\phi = \phi_2 - \phi_1 < const \quad (1)$$

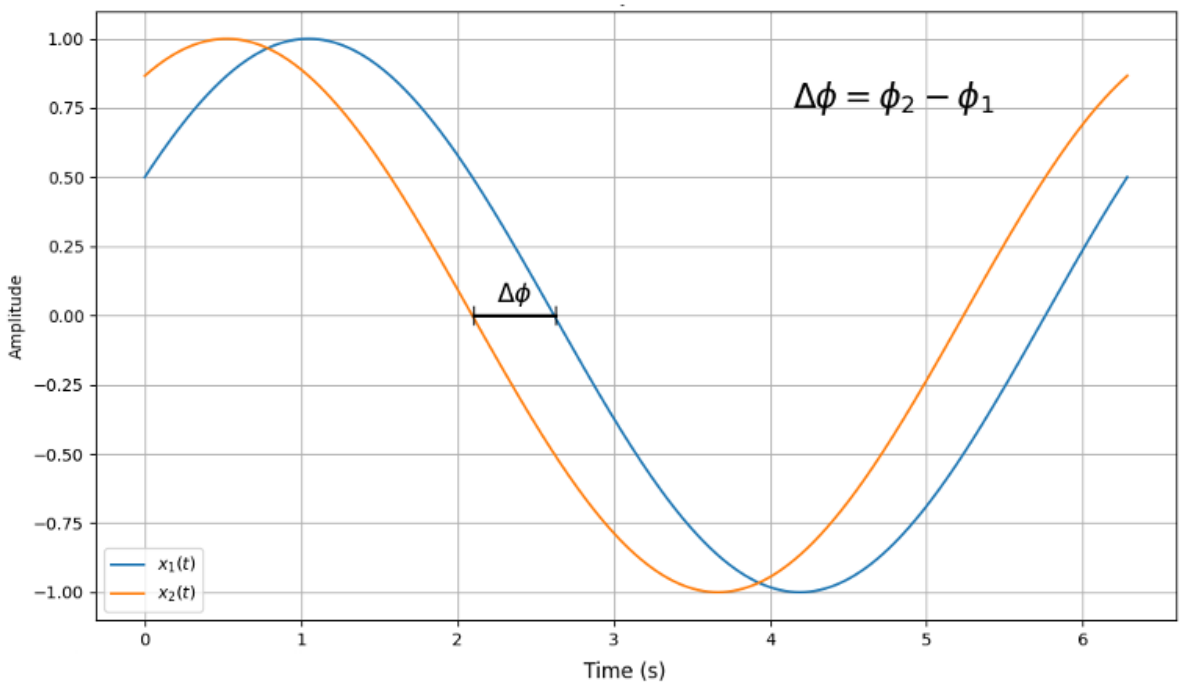

Figure 10. Illustration of the phase difference $\Delta\phi$ of two simulated signals $x_1(t)$, $x_2(t)$.

In order to calculate the instantaneous phase of the signals, we use the Hilbert transform to obtain the analytical signal $z(t)$ which is complex valued with $x(t)$ a real time series and $\hat{x}(t)$ its corresponding Hilbert transform,

$$z(t) = x(t) + i\hat{x}(t) = A(t)e^{i\phi(t)} \quad (2)$$

where the imaginary component is obtained via the following integration:

$$\hat{x}(t) = \frac{1}{\pi} P \int_{-\infty}^{\infty} \frac{x(\tau)}{t-\tau} d\tau \quad (3)$$

where *P* refers to the Cauchy principal value. From Eq. 2, we can determine the signals both instantaneous amplitude A(t) and phase $\phi(t)$ by:

$$A(t) = \sqrt{[x(t)]^2 + [\hat{x}(t)]^2} \text{ and } \quad \phi(t) = arctan\left(\frac{\hat{x}(t)}{x(t)}\right) \qquad (4)$$

The *phase lag index* (PLI) was an idea introduced as a way of estimating phase synchronization that remained unaffected in the presence of common sources such as volume conduction and active reference electrodes (Stam et al., 2007). A way to achieve this is by defining an asymmetry index for the distribution of all phase differences at a given time interval. If the phases are not coupled in any way, this distribution is expected to be flat and centered around zero. Any deviation from this flat distribution indicates some degree of phase synchronization. Lack of symmetry of the $\Delta\phi$ distribution around zero implies that the likelihood that the phase difference will be in the interval $-\pi < \Delta\phi < 0$ is different than the likelihood of it being in the interval $0 < \Delta\phi < \pi$. This asymmetry represents a nonrandom nonzero phase difference between the two signals in that time interval, one that cannot be explained as a consequence of volume conduction from a single source, since these influences affect both signals simultaneously. In the case of no signal coupling, the distribution is expected to be flat, or the median phase difference is expected to be equal to or centered around a value of 0 mod π. It is the latter case in which standard measures of phase synchronization provide large values, while the proposed index provides small ones. For a time series of phase differences, an index of the asymmetry of the distribution can be calculated as follows:

$$PLI \equiv |\langle sgn(\Delta\phi)\rangle| \; where, sgn(\Delta\phi) = \begin{cases} 1 \; if \; \Delta\phi > 0 \\ -1 \; if \; \Delta\phi < 0 \\ 0 \; if \; \Delta\phi = 0 \end{cases} \qquad (6)$$

The PLI value ranges between 0, indicating either no phase coupling or coupling with a phase difference centered around 0 mod π, and 1, indicating perfect phase locking at a value centered around $\Delta\phi$ different from 0 mod π. When estimating the PLI, small signal perturbations can sometimes turn phase lags into leads and vice versa, this hinders the PLI's sensitivity to noise and volume conduction, a problem that becomes more serious for synchronization effects of smaller magnitude. To better detect changes in phase synchronization, Vinck and colleagues (Vinck et al., 2011) proposed an improved index, called the weighted phase-lag index (wPLI), defined as:

$$wPLI \equiv \frac{|\langle |\Delta\phi| \cdot sgn(\Delta\phi)\rangle|}{\langle |\Delta\phi| \rangle} \qquad (7)$$

PLI is especially susceptible to alterations due to noise when the noise source is symmetrically distributed, this is because PLI simply detects whether the phase lag is consistent in one direction, ignoring the magnitude of the phase difference. wPLI, on the other hand, addresses this problem by providing more weight to phase differences that are far from 0 mod π, meaning it puts a larger emphasis on phase differences that are stronger and less likely to be related to noise, reducing false detections of synchronization caused by artifacts. wPLI also improves the handling of volume conduction by further reducing the impact of zero-lag interactions, i.e., more effectively dealing with zero-lag phase relationships caused by volume conduction than PLI alone.

Having chosen wPLI as our preferred method of estimating functional connectivity, for each subject, connectivity matrices were derived for each epoch and frequency band of interest, where each matrix element represented the wPLI value between a pair of EEG channels (Fig. 11). For subsequent statistical analyses, these matrices served as the basis for generating undirected weighted graphs that were utilized for studying and comparing connectivity patterns utilizing metrics defined by graph theory, described in detail in the following section.

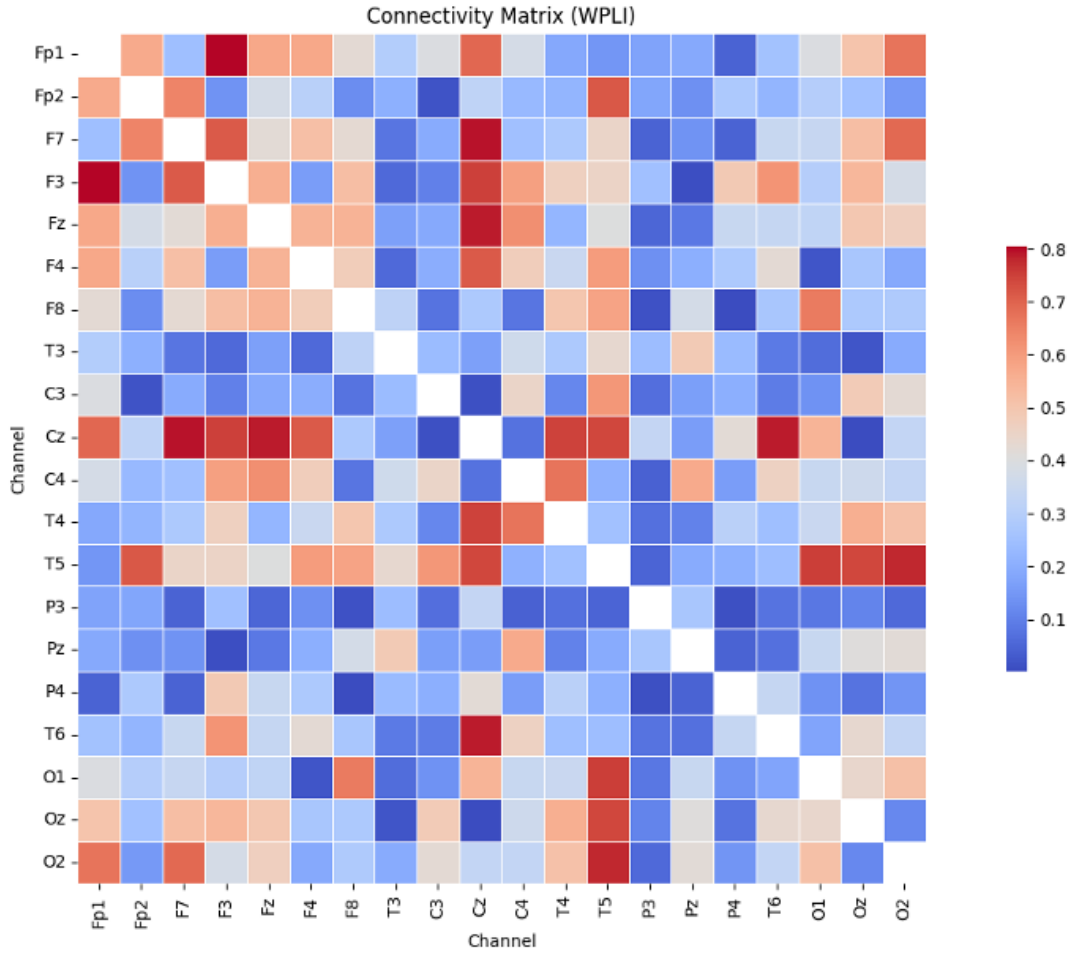

Figure 11. Example of a connectivity matrix derived from applying pairwise wPLI measurements to all electrodes.

2.3.2. Graph Theory

As the field of neuroscience moved away from modeling the brain as a collection of localized functions and towards a more integrative understanding of function emerging from networks formed through the complex interplay and communication of several regions, mathematical tools have emerged to study and quantify these networks properties. One such tool is **graph theory**.

In discrete mathematics, graph theory is used to represent and model pairwise relations between objects through the study of *graphs*, which are mathematical structures made up of *vertices* (also called nodes) which are connected by *edges*. Formally, a graph G is defined as an ordered pair G = (V, E) where V is the set of vertices and E represents the edges between them. These edges may be either directed or undirected, depending on whether the relationship between vertices is mutual (undirected) (Fig. 12B) or directional (directed) (Fig. 12A).

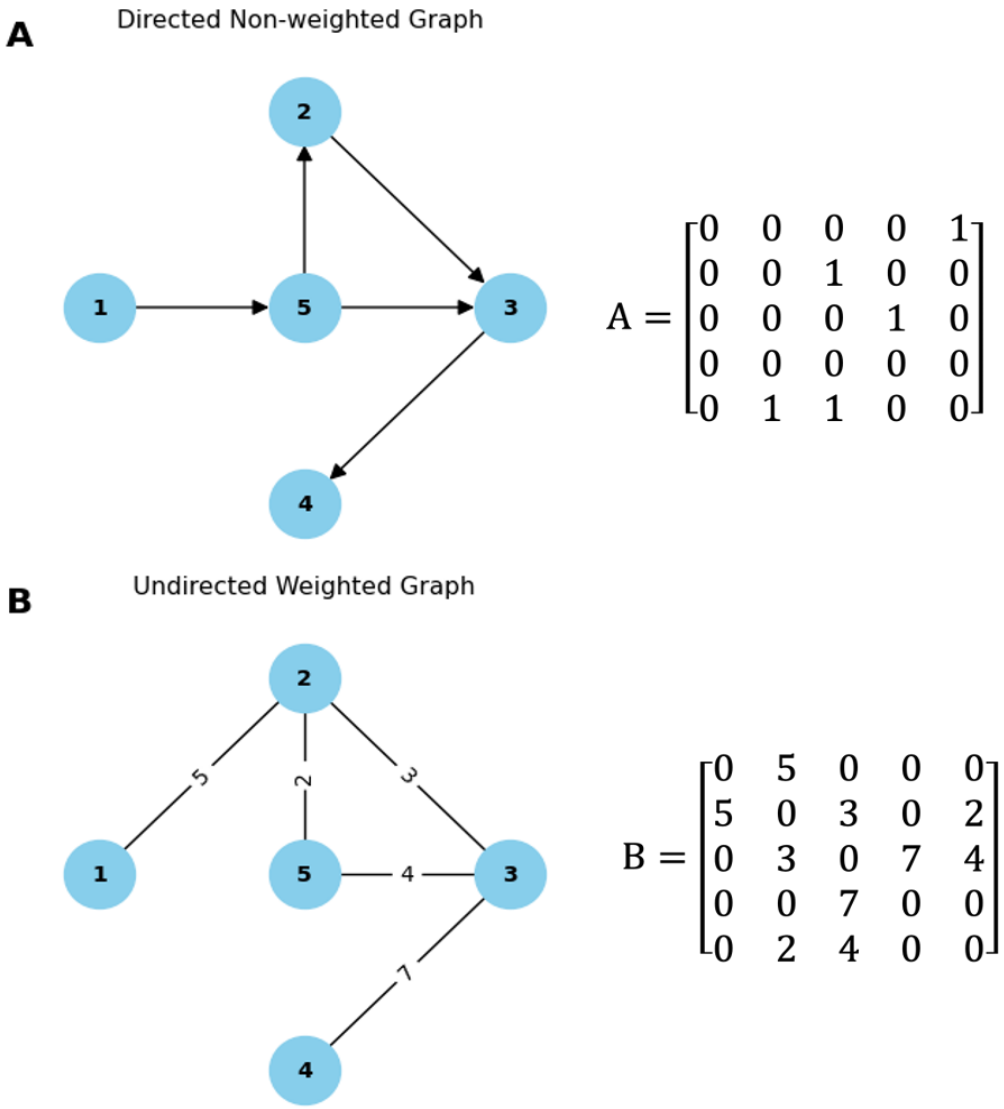

Figure 12. Examples of different graph types and their respective matrices.

Different properties and characteristics give rise to various types of graphs. In undirected graphs, the edges link two vertices in a non-oriented way (e. g., they do not have any direction), whereas directed graphs use an attribute for each edge that specifies the directionality of each vertex. Non-weighted graphs have only binary edges, i.e. they contain only zero or one values, whereas the connections in weighted graphs have weights or values that usually represent the edge's strength and capacity. Graph theory facilitates the investigation of crucial structural properties via *graph metrics,* e.g., degree, centrality, clustering and path-length, each one yielding different information on how networks are organized (topology) on a global and/or local scale.

2.3.3. Common Graph Metrics

Degree. A graph's total number of edges determines its size, and its total number of nodes indicates its order (Bessa A. D., 2010). The number of links that surround every node is equivalent to the degree attribute. The degree of node *i* (d_i) in an undirected binary graph is determined by:

$$d_i = \sum_{i=1}^{N} a_{ij} \tag{8}$$

where N is the total number of nodes and $a_{ij} = 1$ if a link exists between i and j and $a_{ij} = 0$ if not. One can apply the degree to weighted graphs by simply substituting a_{ij} for w_{ij}, where w_{ij} is the weight value for that link.

A graph's mean degree (also called global degree) is just the arithmetic mean of all nodal degrees. In the case of an undirected graph, this implies:

$$\langle d \rangle = \frac{1}{N} \sum_{i=1}^{N} d_i \tag{9}$$

The "degree distribution" is a crucial feature when studying a graph's degree. It displays the likelihood $P(d_i)$ that a that node *i* has degree *d* and can be best visualized in the form of a histogram (Fig. 13).

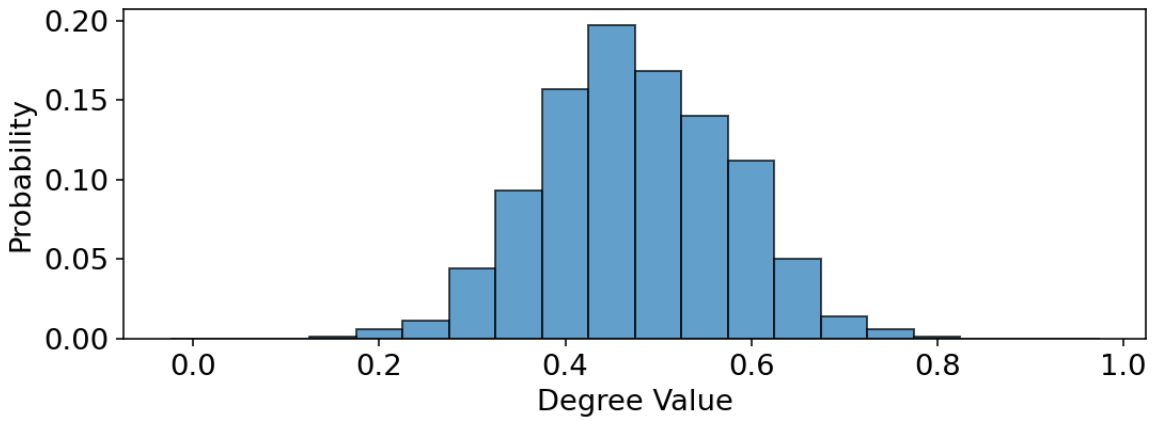

Figure 13. Example of a histogram of a graph's degree distribution.

Characteristic Path-length (efficiency). To understand how efficiently information flows through a graph, one can study the "distance" of a path between two nodes. In an unweighted network, the distance between two vertices is equal to the number of edges in the shortest path that connects them. In a weighted graph, the distance is defined as the sum of the inverse weights along the edges in the shortest path between two vertices, where lower weights imply

larger distances, thus, making nodes with lower weighted connections between them, further apart. The average of all the distances between all pairs of vertices in a network is the typical path length, also known as the average path length. The average of all the reciprocals of the non-zero distances in a network is its global efficiency (Latora & Marchiori, 2001).

Based on this concept, it becomes possible to construct a graph distance matrix (L): a square matrix where each element l_{ij} represents the defined distance between nodes *i* and *j*.

For each node *i*, one can define the average shortest path length by averaging the distance from *i* to every other reachable node in the graph.

$$\langle l_i \rangle = \frac{1}{N} \sum_{j=1}^{N} l_{ij} \tag{10}$$

And the mean value of every l_i represents the network's average shortes path.

$$\langle l \rangle = \frac{1}{N} \sum_{j=1}^{N} l_i \tag{11}$$

From these definitions, it is also useful to define the global efficiency of a network as the average of the inverse of the shortest path lengths between all pairs of nodes in the network:

$$E_{Global} = \frac{1}{N(N-1)} \sum_{i=1}^{N} \frac{1}{l_i} \tag{12}$$

Clustering Coefficient (CC). The CC measures the tendency of nodes to cluster together, i.e. the degree to which nodes in a graph tend to form tightly knit groups characterized by a high density of edges. In an unweighted graph, it provides the probability that the adjacent nodes of a node are connected and can be defined as (Wasserman & Faust, 1994):

$$C = \frac{\#\ of\ closed\ triplets\ connected\ to\ i}{\#\ of\ connected\ triplets\ of\ nodes} \tag{13}$$

Where the numerator counts all instances where three nodes form a closed triangle (closed triplets) and the denominator counts all instances of connected triplets, both open and closed (connected triplets). This ratio provides the probability that the two neighbors of a node are themselves connected, offering a global insight into the network's clustering tendency (Wasserman & Faust, 1994).

In weighted graphs, where edges carry a weigh w_{ij} representing the strength of the connection between nodes *i* and *j*, the clustering coefficient can be extended to incorporate these weights. (Barrat et al., 2004) proposed a weighted clustering coefficient defined as:

$$C_i^w = \frac{1}{s_i(d_i-1)} \sum_{j,h} \frac{(w_{ij}+w_{ih})}{2} a_{ij} a_{jh} a_{hi} \quad (14)$$

where s_i is the **strength** of node *i*, representing the sum of the weights of all edges connected to it, d_i is the node degree, a_{ij} is the element of the adjacency matrix, equal to 1 if nodes *i* and *j* are connected, and 0 otherwise.

2.3.4. EEG-based Functional Networks

EEG records the brain's electrical signals through electrodes in the scalp. Each electrode captures signals from different brain regions and therefore reflects some of the dynamic interactions between those regions. These interactions can best be modeled using a graph-theoretical approach, where each brain region represents a vertex and the edges represent the interactions among these regions, derived from the similarity between their respective EEG signals. Typically, these connections are evaluated using some similarity measure, such as phase–phase synchronization with mutual information or cross-correlation, to assess the functional couplings among different brain areas.

In this context, functional connectivity can be represented as an undirected weighted graph, where how much two brain regions are functionally connected determines the weight of the edge connecting the vertices. A higher phase-synchronization between two EEG signals implies a stronger FC, and therefore, a more heavily weighted edge in the graph.

The graph-theoretical measures defined above may be used in the analysis of EEG data. Brain regions with high degree may be considered as important hubs, which are likely critical for integrating information across different parts of the brain. Another key determinant is the clustering coefficient, which denotes nodes from one group being densely concentrated. High clustering coefficients in EEG-based graphs, for example, are indicative of more localized and synchronous typical work-load level activity emanating from functional brain networks specialized to a certain aspect in cognitive processing (Ismail & Karwowski, 2020). The average path length (efficiency), which is a measure of the mean distance between nodes in the network, is indicative of how efficiently information is transferred through the brain (Thilaga et al., 2018)

Notably, EEG networks often display properties of small-world complex systems characterized by high clustering coefficient and short path length. These small-world properties have been suggested to facilitate locally and globally distributed information processing in the brain supporting successful cognitive function (Liao et al., 2017). Graph metrics extracted from such

graph-based EEG analysis can reveal important information about the abnormalities in brain connectivity that underlies diseases like epilepsy, Alzheimer's disease and schizophrenia. Research of these disruptions and how they impact the communication between different brain areas help shed light on what is happening in those disorders. For example, in epilepsy the graph measures might show that information cannot flow as efficiently or network hubs are reduced (Royer et al., 2022). Similarly, in Alzheimer's disease, the loss of small-world characteristics in the brain's network is often linked to the progressive decline in cognitive abilities (Liu et al., 2012).

3. MATERIALS & METHODS

3.1. Study design and participants recruitment

A cross-sectional and quasi-experimental study design was employed by our collaborators (José Pedro Correia and Sandro Freitas) at the University of Lisbon at the start of the 2021/2022 football season to accomplish the study objectives. The study was advertised among local football male teams. Players with at least five years of football practice, training three times sessions plus a match per week, and with no active injury limiting performance were invited to participate in this study. Players who reported to be goalkeeper, with a history of knee, thigh, hip, or CNS structural injury or surgery, who practiced other sports or structured physical activity twice per week or more in the last 2 years, or who had any condition preventing the player from completing the study protocol were excluded to participate in the study. A total of 124 players (24.3 ± 4.2 years old) were included in the study, 39 (31.4%) of which had a history of HSI in the previous two seasons. All participants provided a consent form before the tests, and this study was approved by the Ethics Committees of both Portugal (#15/2021) and Brazil (CEP nº 0168/2024**)**.

3.2. Protocol

Upon arrival, individuals completed anthropometric and clinical screening and performed a 5-minute warm-up on a stationary bicycle (Ergomedic 828E, Monark) at approximately 70 revolutions per minute. Following the warm-up, individuals were familiarized with the maximum knee flexion/extension movement rate task in a prone position, which has been described previously (Correia et al., 2024). Individuals were given the necessary time to familiarize themselves with the correct range of movement and to demonstrate being able to perform the required range at full speed for a few seconds. Participants were instructed to perform alternating repeated flexion/extension movements with both legs as fast as they could between 45° and 90° of knee flexion (Fig. 14A). The task consisted of eight 10-second blocks of fast bilateral alternating knee flexion/extension movements with a 5-second rest between blocks. The 10-s duration was chosen since this period has been found to show the greatest decrease in movement rate (Bächinger et al., 2019). Verbal encouragement was provided during the task in order to ensure a maximum effort.

3.3. Clinical anamnesis

A sports physiotherapist with more than 10 years of professional practice enquired all participants regarding their demographic, injury, and football-related data. Regarding the hamstring injuries specifically, information on the date of injury occurrence, context, mechanism, time loss (until return to play), time since injury, and injured limb were obtained. A retrospective period of two seasons has previously been used in studies of football-related HSIs (Røksund et al., 2017; Schuermans et al., 2014). Additionally, the accuracy of hamstring injury self-reporting has been previously confirmed (Gabbe et al., 2003). Nevertheless, when possible, the club's clinical department was asked to validate the information.

3.4. Brain electrical activity

EEG data were collected during the whole task using a Vertex SC823 device (Meditron Eletromedicina Ltda, São Paulo, Brazil) (Fig. 14C). Cz alignment was performed using the midpoints of the inion and nasion in the sagittal plane and the two preauricular points in the coronal plane as reference, with the remaining electrodes placed according to the international 10–20 system. A total of 24 channels were used. Online referencing to two mastoid electrodes was performed and the sampling rate was 250 Hz. A circuit impedance of 10 kΩ was ensured in all electrodes prior to starting data collection and a 0.1-70 Hz analog band-pass filter was applied by the amplifier.

3.5. Data analysis

Injury severity and time since injury

Demographic and football-related data were obtained from players, including height, weight, playing position, HSI history in the previous two seasons, time loss due to HSIs, and time since injury. We defined an injury severity index as the injury severity score minus the number of days since the injury times an arbitrary constant (C).

$$Severity\ Index\ =\ Severity\ Score\ -\ C * Days\ since\ Injury \quad (15)$$

Where the injury severity score is defined using the number of days lost due to injury (i.e., without being able to train/play) as: 1: minimal, 1-3 days; 2: mild, 4-7 days; 3: moderate, 8-28 days; 4: severe, >28 days (Fuller et al., 2006).

EEG

The EEG signal underwent preprocessing using the HAPPILEE pipeline, a standardized software for low density EEG data processing (Lopez et al., 2022). 50-Hz line noise reduction was performed using the CleanLine method. Subsequently, data were filtered with a 1-100 Hz bandpass filter using EEGLAB's FIR filter, ensuring the removal of slow drifts and fast noise components. Bad channel detection was enabled and executed, also with EEGLAB, prior to wavelet thresholding to identify and eliminate channels that might introduce noise. The pipeline also incorporated wavelet thresholding with default settings to denoise the EEG signals in the time-frequency domain. The MuscIL feature of HAPPE (Gabard-Durnam et al., 2018) was utilized to specifically address and remove muscle artifacts that frequently contaminate EEG recordings. Finally, the EEG data were re-referenced to the average of all electrodes, a standard procedure that offers a neutral reference and improves the clarity of the EEG signal.

Functional Connectivity (FC). Pairwise connectivity metrics were calculated for all electrodes for each epoch in the following frequency bands: theta (4-7 Hz), alpha (8-13 Hz) and beta (13-30 Hz). In this analysis, we employed the wPLI to estimate the FC between the neural activity of each brain region. Connectivity matrices were derived for each individual and epoch, where each matrix element represented the wPLI value between a pair of EEG channels. For subsequent statistical analyses, these matrices served as the basis for generating undirected weighted graphs that were utilized for comparing connectivity patterns both within and between the control and injured groups.

Graph Analysis. Initially, we analyzed three graph metrics—efficiency, degree, and clustering coefficient. However, we found that for a fully connected weighted graph, efficiency and degree were highly correlated, effectively representing the same metric. Additionally, in the context of our research, the clustering coefficient proved challenging to interpret and yielded convoluted results. Consequently, we chose to focus solely on the degree metric for its simplicity and ease of interpretability. The degree can be assessed both globally (average degree across all nodes in the network) and locally (single node degree or average degree across a subselection of nodes), providing a comprehensive perspective of the graph's topology. We calculated the rest and activity degrees for each node by averaging the degree values across corresponding epochs. The degree difference was determined by calculating the average percent change in degree for each transition from a rest to an activity epoch. For our subnetwork analysis, we grouped individual nodes into predefined networks, as illustrated in Fig. 14B.

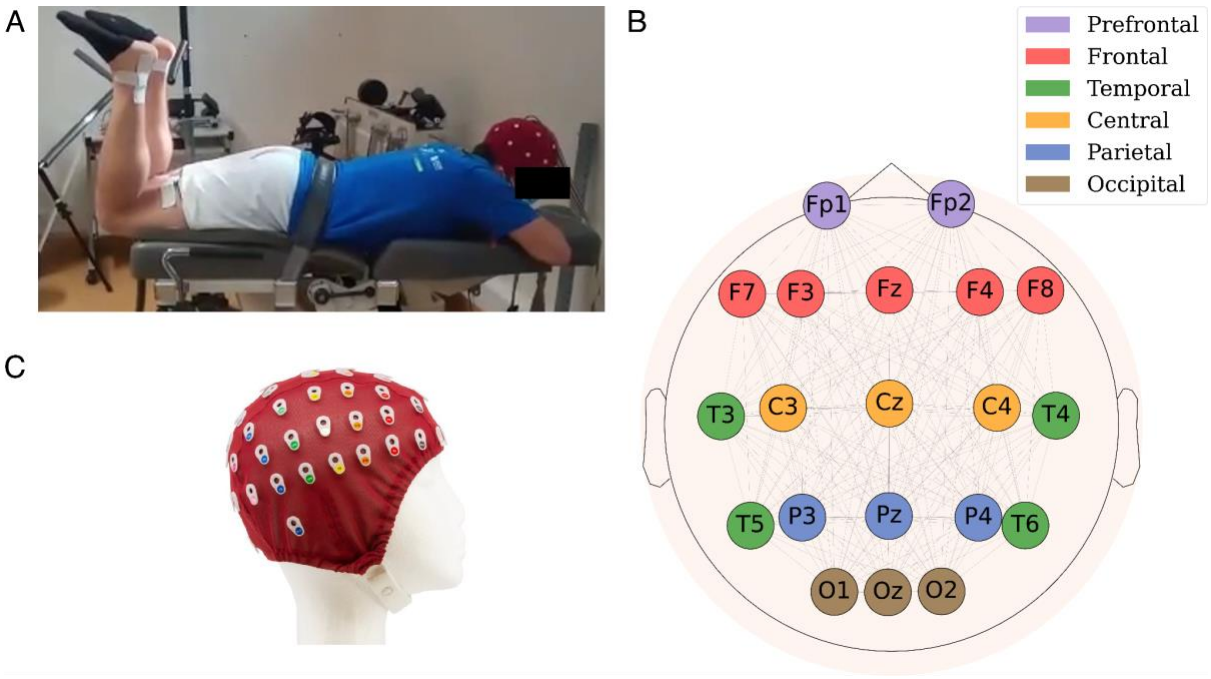

Figure 14. Experimental setup and electrodes layout. (A) Photo of the experimental setup utilized in the motor task protocol employed in the study. (B) Illustration of the electrode layout showing the electrode grouping into different networks used for statistical analysis. (C) Detailed view of the EEG cap utilized in the experiment.

Statistical Analysis

All statistical analyses were conducted using Python libraries such as SciPy and Statsmodels. A two-way mixed ANOVA [2 (HSI, No HSI) x 2 (activity, rest)] was conducted to compare the global degree between injured athletes and the control group for each frequency band of interest (theta, alpha, beta). To identify spatial characteristics and differences between groups, a two-way mixed ANOVA [2 (HSI, Control) x 6 subnetworks] was conducted to compare local degree changes across six subnetworks (frontal, prefrontal, parietal, central, occipital, temporal) and between the injured and control groups. A partial correlation analysis was conducted to examine the relationship between four injury parameters (severity score, time since injury, time loss due to injury and severity index) and global degree change, as well as degree changes across all subnetworks in the alpha band, while controlling for task performance (TP) and reported fatigue (RF) among injured individuals. Bonferroni correction was applied for multiple comparisons, with significance set at $p < 0.05$. Effect sizes were calculated using partial eta squared (η_p^2) values and classified as small (0.01-0.06), medium (0.06-0.14), or large (>0.14) (Richardson, 2011).

4. RESULTS

A total of 124 subjects participated in the study, of which 21 goalkeepers were excluded and 4 did not complete the experimental task. After preprocessing the data, 10 subjects did not meet a satisfactory signal to noise ratio and were excluded due to excessive noise in the EEG recordings. The following analysis was conducted with the remaining 89 subjects (24.1 ± 4.0 years old, 30 injured, 59 control).

4.1. Task-Related Functional Connectivity Changes

Performing the knee flexion-extension task was generally associated with a significant decrease in global degree at the alpha band during activity compared to rest for both groups (HSI: $p<0.0001$, $\eta_p^2 = 0.38$, control: $p = 0.0003$, $\eta_p^2 = 0.11$; Fig. 15A). This decrease was consistent across regions, with no significant differences observed between them ($p > 0.05$), and it did not correlate with task performance or reported fatigue. We found no significant differences in the theta and beta frequency bands (Fig. A3 & Fig. A4).

4.2. Group Differences: HSI vs. Control

When comparing the injured and control groups, there was a significant difference in the percentage change in global degree from rest to activity, with the injured group showing a greater decrease in connectivity ($p = 0.0006$, $\eta_p^2 = 0.13$; Fig. 15B). For the rest epochs, there were no significant differences between groups ($p = 0.2$, $\eta_p^2 = 0.02$; Fig. 15A), whereas for the activity epochs, the injured group presented a significantly lower connectivity ($p = 0.006$, $\eta_p^2 = 0.07$; Fig. 15A). When comparing the sub-networks, we found that the injured group presented a significantly greater decrease in connectivity in the frontal ($p = 0.0004$, $\eta_p^2 = 0.17$; Fig. 15C) and temporal ($p = 0.03$, $\eta_p^2 = 0.08$; Fig. 15C) regions when compared to the control group.

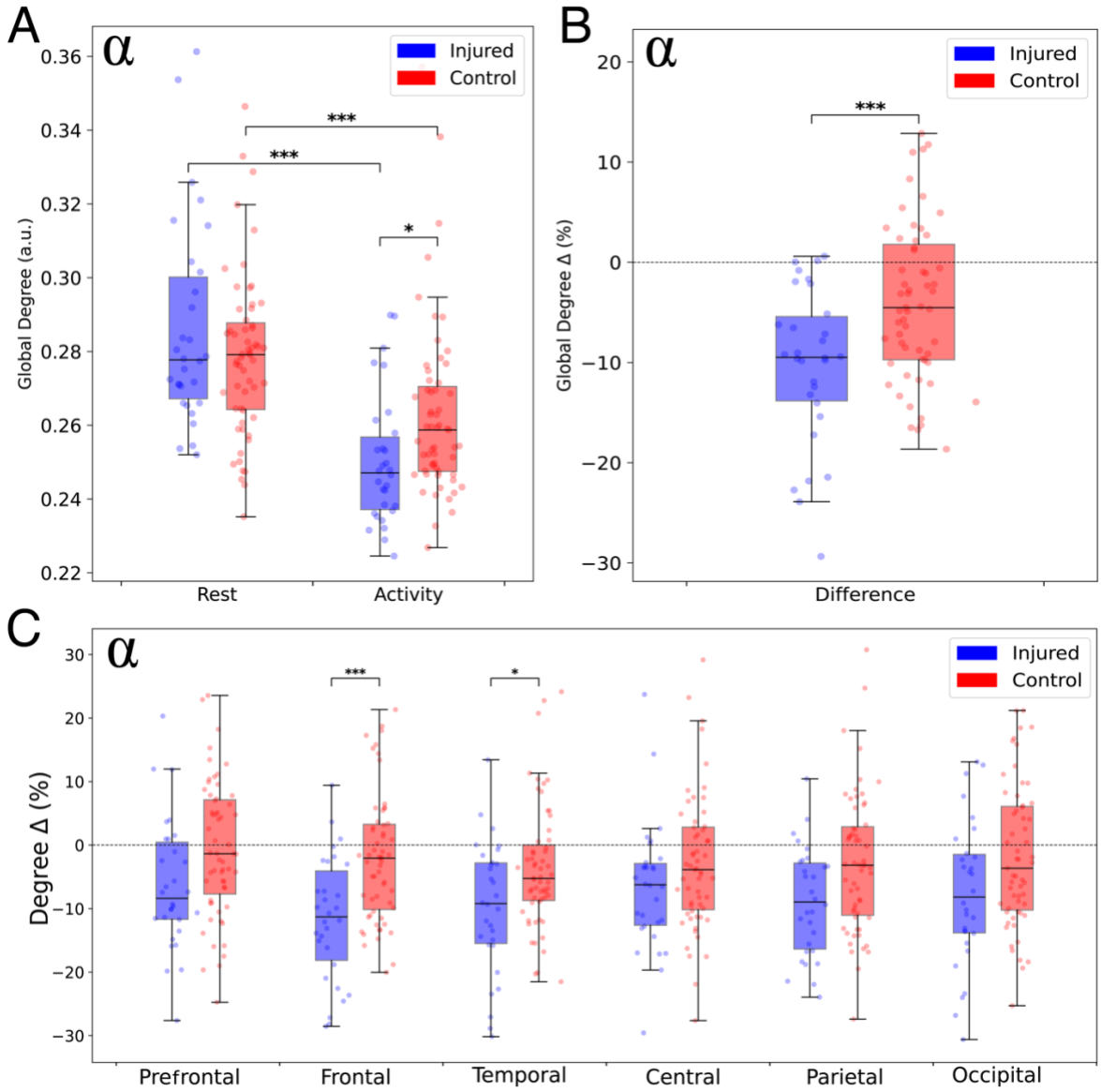

Figure 15. Group comparisons of brain FC at alpha. (A) Boxplot comparing the global degree between activity and rest epochs for both injured (blue) and control (red) groups. (B) Boxplot comparing the percent change in global degree when transitioning from rest to activity for both groups. (C) Boxplot comparing the percent change in local degree for each of the 6 networks for both groups. (Asterisks indicate statistical significance: ***$p < 0.001$, **$p < 0.01$, *$p < 0.05$)

4.3. Injury Parameters Correlations

A partial correlation analysis was conducted to examine the relationship between the graphs' global and local degree in the alpha band and 4 injury parameters: days away due to injury, days since injury, severity score, and the injury severity index, while controlling for task performance, reported fatigue and age among the injured group. No significant correlation was found between global degree change and days away due to injury (p=1, r=-0.14, Fig. 16A) and days since injury (p=1, r=0.16, Fig. 16B). However, significant negative correlations were observed between global degree change and the severity score (p=0.023, r=-0.49, Fig. 16C) and the injury severity index (p=0.003, r=-0.58, Fig. 16D). The most significant correlations were found in the prefrontal (severity score: p=0.045, r=-0.54; severity index: p=0.077, r=-0.52), frontal (severity score: p=0.14, r=-0.49; severity index: p<0.001, r=-0.72) and parietal regions (severity score: p=0.011, r=-0.60; severity index: p=0.015, r=-0.59). All the results are summarized in Table 2.

Table 2. Results from the partial correlation analysis of injury parameters and network degree changes at alpha. Each cell represents the correlation results in the format: [r-value, CI95%, p-value]. Bold cells contain significant p-values (p<0.05).

	Days away due to injury	Days since injury	Severity Score	Severity Index
Global	[-0.14, (-0.48, 0.23), 1]	[0.16, (-0.21, 0.49), 1]	**[-0.49, (-0.72, -0.16), 0.023*]**	**[-0.58, (-0.78,-0.28), 0.003**]**
Prefrontal	[-0.15, (-0.48, 0.22), 1]	[0.08, (-0.29, 0.43), 1]	**[-0.54, (-0.76, -0.23), 0.045*]**	[-0.52, (-0.74, -0.2), 0.077]
Frontal	[-0.12, (-0.46, 0.25), 1]	[0.33, (-0.04, 0.61), 1]	[-0.49, (-0.72, -0.16), 0.139]	**[-0.72, (-0.86, -0.49), 0.00016***]**
Parietal	[-0.4, (-0.67, -0.05), 0.66]	[-0.01, (-0.37, 0.35), 1]	**[-0.6, (-0.79, -0.3), 0.011*]**	**[-0.59, (-0.78, -0.29), 0.015*]**
Central	[-0.19, (-0.51, 0.18), 1]	[0.09, (-0.28, 0.44), 1]	[-0.36, (-0.64, 0.0), 1]	[-0.37, (-0.65, -0.02), 1.00]
Temporal	[0.11, (-0.26, 0.45), 1]	[0.14, (-0.23, 0.47), 1]	[-0.15, (-0.49, 0.22), 1]	[-0.27, (-0.58, 0.1), 1]
Occipital	[-0.03, (-0.39, 0.33), 1]	[0.26, (-0.11, 0.57), 1]	[-0.27, (-0.58, 0.1), 1]	[-0.41, (-0.67, -0.06), 0.55]

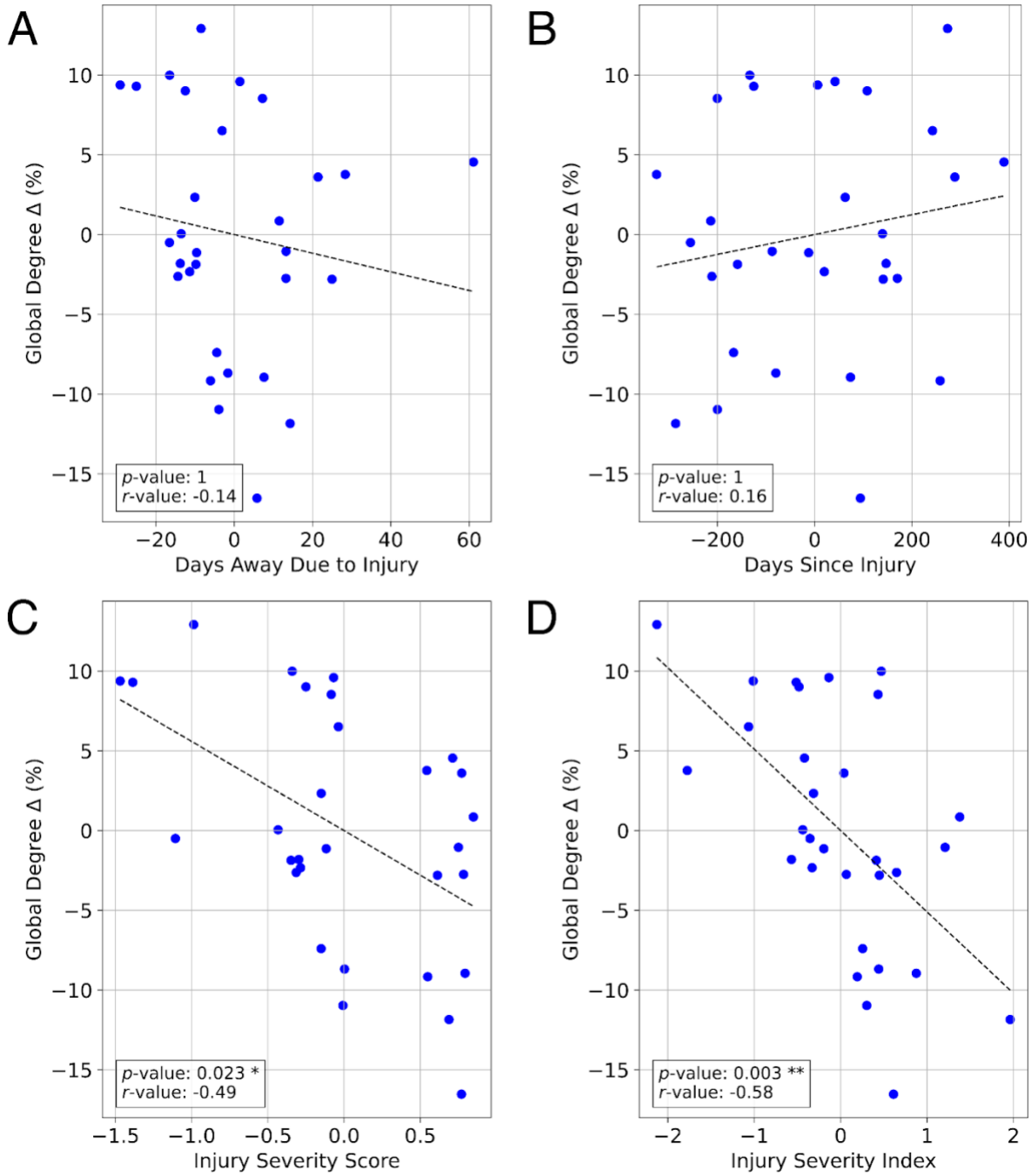

Figure 16. Linear fit between global FC change at alpha and regressed residuals of clinical parameters. Graphs of the linear fits between percent global degree change at alpha and the regressed residuals of (A) days away due to injury, (B) days since injury, (C) injury severity score and (D) injury severity index.

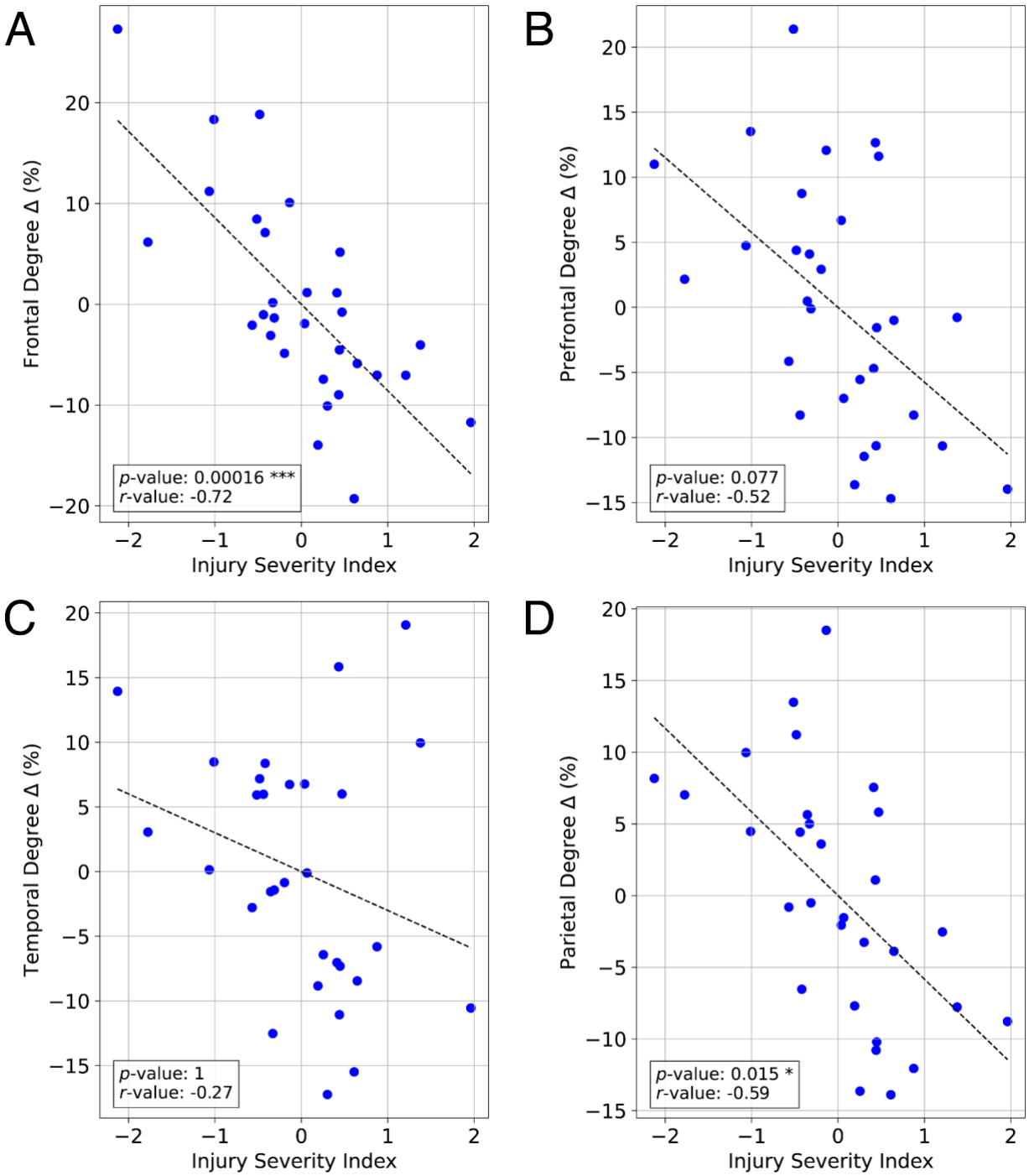

Figure 17. Linear fit between the regressed residuals of the injury severity index and network FC change at alpha. Graphs of the linear fits between the regressed residuals of the injury severity index and the (A) frontal, (B) prefrontal, (C) temporal and (D) parietal percent degree change at alpha.

5. DISCUSSION

The present study analyzed EEG-based FC variations between injured and control athletes during fast bilateral alternating knee flexion/extension movements, focusing on global and local degree metrics in the alpha band across activity and rest epochs. To the best of our knowledge, this is the first time that this type of analysis has been made within this population. While our study primarily focused on the alpha band due to its established role in motor tasks and its significant findings related to HSIs, we also analyzed other frequency bands. Despite previous findings relating motor function and injury to theta and beta oscillations using power analysis (Baumeister et al., 2008; Zhang et al., 2022), we did not encounter any significant changes in these frequency bands in our analysis. This absence of significant findings in the theta and beta bands suggests that alpha oscillations may play a more prominent role in the FC changes associated with HSIs during high-speed knee movement.

5.1. Alpha Connectivity Reduction During Motor Activity

The main FC trend observed in our study was a significant decrease in global degree during activity compared to rest for both groups in the alpha frequency band (Fig. 15A), indicating a widespread reduction in alpha connectivity associated with motor activity. Studies commonly refer to a reduction in alpha power during motor tasks as "alpha desynchronization", a phenomenon indicative of cortical activation (Neuper & Pfurtscheller, 2001). This desynchronization occurs during motor actions, such as imagining or executing movements, and is thought to reflect the engagement and activation of sensorimotor areas necessary for the planning and execution of motor activities (Di Nota et al., 2017; Fink et al., 2018; Ulanov & Shtyrov, 2022).

Research has consistently demonstrated that alpha desynchronization is a reliable marker of motor preparation and execution. For instance, Di Nota et al. (2017) highlighted the role of alpha desynchronization in the modulation of sensorimotor rhythms during action observation and motor imagery. Similarly, Ulanov and Shtyrov (2022) found that alpha power reductions are closely associated with motor task performance, underscoring the link between alpha desynchronization and motor activity. These studies use "alpha desynchronization" to reference a reduction in alpha power. While this does not mean the same thing as an alpha connectivity reduction, the two events are likely very much related.

Our study's findings of reduced alpha connectivity therefore likely reflect similar neural mechanisms as those observed in the studies on alpha desynchronization. The observed reduction in global degree during the execution of knee flexion/extension movements suggests the activation of motor-related brain regions. Although alpha desynchronization is expected to be more pronounced in the prefrontal and central regions, where the motor cortex is located, we did not find significant spatial characteristics in our study. This lack of spatial specificity might be attributed to the low spatial resolution of the EEG recordings used, which may not adequately capture the finer details of localized brain activity during motor tasks.

These findings provide a broader understanding of how alpha connectivity reduction during motor activities might relate to previously documented phenomenon of alpha desynchronization, further linking functional connectivity changes to cortical activation in the context of motor tasks. They also contribute to our understanding of how injuries impact brain function during motor activities and underscore the importance of considering both global and regional changes in connectivity.

5.2. Differences in Connectivity Between HSI and Control Groups

The injured group exhibited a significantly greater decrease in global alpha connectivity compared to the control group. When examining the global degree during rest and activity, there was a significant difference only during the activity phase, indicating that the observed differences were predominantly due to FC variations during the execution of the motor task.

In the subnetworks analysis, the most significant group differences were in the prefrontal and temporal regions. The prefrontal cortex is crucial for motor planning and movement sequencing, decision-making, and cognitive control, while the temporal cortex includes part of the sensorimotor region, which is involved in processing sensory information and integrating it with motor commands (Edwards et al., 2019; Pape & Siegel, 2016). Decreased alpha power and FC has been associated with increased perceived mental workload and task demands/complexity (Raufi & Longo, 2022; Shaw et al., 2019) The reported mechanisms behind this decreased connectivity include a top-down reduced cortical disinhibition as a response to the need to allocate additional resources to task performance (e.g., attentional, visuospatial, and sensorimotor coordination resources) (Shaw et al., 2019). In this sense, our findings of decreased alpha FC in footballers with HSI history may mean that these players need to use more cortical resources to cope with the demands of this maximal task.

Two mechanisms may be behind these differences; either players with HSI history show a lower neural efficiency (whether pre- or post-injury), and therefore allocate more cortical processing resources to a given task, or the injury led to the need to dedicate more attention to spatiotemporal joint parameters during task execution due to the greater reliance on top-down (internal motor programs) rather than on bottom-up (peripheral proprioceptive afferences). Existing evidence suggests that alpha cortical communication is decreased in less proficient motor performance (Babiloni et al., 2011; Del Percio et al., 2011). However, previously injured players actually showed greater performance, so this association between alpha FC and task performance is unlikely to explain our findings, also considering the lack of correlation between task performance and alpha global degree decrease. It therefore seems more likely that the increased workload shown by these players is due to the need to allocate more resources (perhaps for sensorimotor integration and monitoring of joint parameters) to cope with task demands. This is supported by the fact that differences were only seen during activity and were most evident in regions associated with motor planning and control. In any case, this greater resource use inevitably leads to a lower motor-cognitive reserve, thus decreasing the ability to cope with additional and/or unexpected demands during athletic performance (Kamijo et al., 2007), which potentially increases the injury risk.

5.3. Alpha Connectivity and Injury Parameters Correlations

Given our hypothesis that the injury severity and the time since the injury event until the data acquisition would have an impact on the measured FC differences, we proposed a model to encompass both these effects in a single measure: the injury severity index (Section 2.4). This hypothesis was based on the assumption that more severe injuries would result in greater alterations in FC, while a longer time since the injury would diminish these effects. Our analysis revealed that the injury severity index demonstrated stronger correlations with the percent global degree change compared to any single metric alone (Fig. 16), suggesting that this combined measure serves as a more accurate predictor of the injury's impact on alpha connectivity. Interestingly, while the correlation between global degree change and days since injury alone was not significant ($p > 0.05$), it was the only metric to show a positive correlation, indicating that more time since the injury indeed correlates with a lesser effect on FC (Fig. 16B).

If, as suggested by Di Trani (2017), HSIs damage mechanoreceptors and lead to cortical adaptations, then more severe and/or recent injuries would induce more damage and cause

greater sensorimotor integration difficulty (Roussiez & Van Cant, 2019). This increased difficulty would, in turn, require a greater allocation of cortical resources to monitor task performance, as reflected by the more pronounced decrease in alpha FC.

This proposed model of increased cortical resource allocation following HSIs is supported by our finding that this correlation was most significant in the frontal and parietal networks (Fig. 17A & 17D). The frontal network corresponds primarily to the premotor cortex, a region responsible for not only the selection, planning and execution of movement (Caminiti et al., 1991) but also for cognitive functions such as spatial attention and working memory (Simon et al., 2002). The parietal network is mainly comprised of the superior parietal lobe, a region thought to be essential for sensorimotor integration and for maintaining internal representations of the body's current state (Wolpert et al., 1998). Studies have shown that sensory and motor deficits can emerge from lesions in this area, underscoring its role in integrating sensory and motor signals (Freund, 2001; Wolpert et al., 1998). Overall, the key functions of the main affected regions strongly support the hypothesis that the greater alpha FC reduction seen in the HSI group reflects an increased cognitive effort requirement for motor planning and sensorimotor integration during the execution of the motor task due to injury.

Alternatively, it is possible that individuals with naturally higher working memory demands during motor activity are more susceptible to injuries. This hypothesis aligns with research suggesting that variations in neural activity and connectivity can influence an individual’s susceptibility to injury, as neural mechanisms play a crucial role in maintaining motor coordination and stability (Criss et al., 2020; Diekfuss et al., 2019, 2020). Further research is needed to explore this potential bidirectional relationship and to determine whether alpha connectivity reduction during motor activity can be used as a predictive marker for injury risk.

5.4. Study Limitations

While our study provides valuable insights into the impact of HSIs on brain FC in professional soccer players, several limitations must be acknowledged. Firstly, the cross-sectional design of the study limits our ability to draw causal inferences about the relationship between HSIs and changes in FC. Longitudinal studies are needed to establish temporal relationships and track changes over time. Secondly, the relatively small sample size may limit the generalizability of our findings to the broader population of athletes. Future studies with larger cohorts are

necessary to validate and extend our results. Thirdly, the use of EEG, while providing high temporal resolution, brings limited spatial resolution compared to other neuroimaging techniques such as fMRI. This limitation may affect the precision of localization of cortical changes. Lastly, self-reported injury history may be subject to recall bias, which could impact the accuracy of the injury severity data. Addressing these limitations in future research will be crucial for deepening our understanding of the neural consequences of HSIs and enhancing injury management strategies.

6. CONCLUSION

For the first time, we have measured electrical cortical activation patterns during the execution of a motor task and were able to detect the influence of an HSI on brain-wide and network specific FC parameters. In addition to impairing physical ability, HSIs, known for their high recurrence rates and debilitating effects on performance, can also induce proprioceptive deficits and modifications in the corticomotor organization. Based on our findings, we suggested that the globally reduced alpha connectivity in injured athletes during motor tasks reflects an increase in the cognitive effort required to perform the task due to the injury. Considering this model of HSI, subsequent studies should include sensory inputs and decision-making components to the motor task, designed to manipulate the working memory load and validate or refute the proposed model.

Moreover, we proposed an injury severity index, which significantly correlated with FC changes, outperforming any other metric alone, underlining how both the severity and recency of the HSI play an important role at determining the magnitude of the disruption of normal cortical functions. These correlations were most significant in the frontal and parietal networks, suggesting that HSIs might mainly affect functions such as motor planning and sensorimotor processing. This underlines the importance for rehabilitation protocols to address both the physiological and neurological aspects of recovery. As we deepen our understanding of the multifaceted relationship between musculoskeletal injuries and brain activity, we can develop better interventions to improve recovery and prevent re-injury.

Future research should incorporate longitudinal study design, as it would be invaluable to determine the directionality of the observed relationship between HSI and increased cognitive effort, determining whether HSIs cause an increase in the required cognitive load, or whether athletes who naturally exhibit a higher cognitive demand are more susceptible to these injuries. Resolving these questions would represent one step further in the direction of using EEG-based connectivity analysis as a tool for developing targeted rehabilitation protocols and injury prevention strategies tailored to the cognitive profile of each athlete.

REFERENCES

Andrea Di Trani. (2017). *Neuromechanical contributions to hamstring stiffness dysregulation and injury*.

Angrisani, L., Arpaia, P., & Casinelli, D. (2017). Instrumentation and measurements for non-invasive EEG-based brain-computer interface. *2017 IEEE International Workshop on Measurement and Networking (M&N)*, 1–5. https://doi.org/10.1109/IWMN.2017.8078383

Avanzini, P., Fabbri-Destro, M., Dalla Volta, R., Daprati, E., Rizzolatti, G., & Cantalupo, G. (2012). The Dynamics of Sensorimotor Cortical Oscillations during the Observation of Hand Movements: An EEG Study. *PLoS ONE*, *7*(5), e37534. https://doi.org/10.1371/journal.pone.0037534

Azevedo, F. A. C., Carvalho, L. R. B., Grinberg, L. T., Farfel, J. M., Ferretti, R. E. L., Leite, R. E. P., Filho, W. J., Lent, R., & Herculano-Houzel, S. (2009). Equal numbers of neuronal and nonneuronal cells make the human brain an isometrically scaled-up primate brain. *Journal of Comparative Neurology*, *513*(5), 532–541. https://doi.org/10.1002/cne.21974

Babiloni, C., Infarinato, F., Marzano, N., Iacoboni, M., Dassù, F., Soricelli, A., Rossini, P. M., Limatola, C., & Del Percio, C. (2011). Intra-hemispheric functional coupling of alpha rhythms is related to golfer's performance: A coherence EEG study. *International Journal of Psychophysiology*, *82*(3), 260–268. https://doi.org/10.1016/j.ijpsycho.2011.09.008

Bächinger, M., Lehner, R., Thomas, F., Hanimann, S., Balsters, J., & Wenderoth, N. (2019). Human motor fatigability as evoked by repetitive movements results from a gradual breakdown of surround inhibition. *ELife*, *8*. https://doi.org/10.7554/eLife.46750

Barrat, A., Barthélemy, M., Pastor-Satorras, R., & Vespignani, A. (2004). The architecture of complex weighted networks. *Proceedings of the National Academy of Sciences*, *101*(11), 3747–3752. https://doi.org/10.1073/pnas.0400087101

Bastos, A. M., & Schoffelen, J.-M. (2016). A Tutorial Review of Functional Connectivity Analysis Methods and Their Interpretational Pitfalls. *Frontiers in Systems Neuroscience*, *9*. https://doi.org/10.3389/fnsys.2015.00175

Baumeister, J., Reinecke, K., Schubert, M., & Weiß, M. (2011). Altered electrocortical brain activity after ACL reconstruction during force control. *Journal of Orthopaedic Research*, *29*(9), 1383–1389. https://doi.org/10.1002/jor.21380

Baumeister, J., Reinecke, K., & Weiss, M. (2008). Changed cortical activity after anterior cruciate ligament reconstruction in a joint position paradigm: an EEG study. *Scandinavian Journal of Medicine & Science in Sports*, *18*(4), 473–484. https://doi.org/10.1111/j.1600-0838.2007.00702.x

Beltramini, G. C. (2014). Análise temporal de correlatos hemodinâmicos associados à atividade epileptiforme através da técnica de EEG-RMf simultâneos. *UNICAMP*.

Bessa A. D., S. L. B. L. , M. L. P. N. R. , C. M. C. , C. P. G. S. (2010). Introdução às Redes Complexas. *Https://Www.Dpi.Inpe.Br/Geocxnets/Wiki/Lib/Exe/Fetch.Php?Media=wiki:Introducao_as_redes_complexas.Pdf*.

Bigbee, J. W. (2023). *Cells of the Central Nervous System: An Overview of Their Structure and Function* (pp. 41–64). https://doi.org/10.1007/978-3-031-12390-0_2

Buzsáki, G., Anastassiou, C. A., & Koch, C. (2012). The origin of extracellular fields and currents — EEG, ECoG, LFP and spikes. *Nature Reviews Neuroscience*, *13*(6), 407–420. https://doi.org/10.1038/nrn3241

Cameron, M., Adams, R., & Maher, C. (2003). Motor control and strength as predictors of hamstring injury in elite players of Australian football. *Physical Therapy in Sport*, *4*(4), 159–166. https://doi.org/10.1016/S1466-853X(03)00053-1

Caminiti, R., Johnson, P. B., Galli, C., Ferraina, S., & Burnod, Y. (1991). Making arm movements within different parts of space: the premotor and motor cortical representation of a coordinate system for reaching to visual targets. *J. Neurosci.*, *11*(5), 1182–1197.

Cavaleri, R., Imam, J., Rio, E., Moukhaiber, N., Thomson, D., Suhood, A., & Summers, S. J. (2023). Investigating interindividual variability in corticomotor reorganization during sustained hamstring pain: A randomized experimental study. *Brain and Behavior*, *13*(5). https://doi.org/10.1002/brb3.2996

Chen, X., Chiang, J., Wang, Z. J., Mckeown, M. J., & Ward, R. K. (2016). Removing muscle artifacts from EEG data: Multichannel single-channel techniques? *IEEE Sens. J*, *16*, 1986–1997.

Correia, J. P., Domingos, C., Witvrouw, E., Luís, P., Rosa, A., Vaz, J. R., & Freitas, S. R. (2024). Brain and muscle activity during fatiguing maximum-speed knee movement. *Journal of Applied Physiology*, *136*(1), 200–212. https://doi.org/10.1152/japplphysiol.00145.2023

Criss, C. R., Onate, J. A., & Grooms, D. R. (2020). Neural activity for hip-knee control in those with anterior cruciate ligament reconstruction: A task-based functional connectivity analysis. *Neuroscience Letters*, *730*, 134985. https://doi.org/10.1016/j.neulet.2020.134985

Darracq, M., Funk, C. M., Polyakov, D., Riedner, B., Gosseries, O., Nieminen, J. O., Bonhomme, V., Brichant, J.-F., Boly, M., Laureys, S., Tononi, G., & Sanders, R. D. (2018). Evoked Alpha Power is Reduced in Disconnected Consciousness During Sleep and Anesthesia. *Scientific Reports*, *8*(1), 16664. https://doi.org/10.1038/s41598-018-34957-9

Del Percio, C., Iacoboni, M., Lizio, R., Marzano, N., Infarinato, F., Vecchio, F., Bertollo, M., Robazza, C., Comani, S., Limatola, C., & Babiloni, C. (2011). Functional coupling of parietal alpha rhythms is enhanced in athletes before visuomotor performance: a coherence electroencephalographic study. *Neuroscience*, *175*, 198–211. https://doi.org/10.1016/j.neuroscience.2010.11.031

Delorme, A. and S. M. (2004). EEGLAB: an open source toolbox for analysis of single-trial EEG dynamics including independent component analysis. *Journal of Neuroscience Methods*, *134.1*, 9–21.

Di Nota, P. M., Chartrand, J. M., Levkov, G. R., Montefusco-Siegmund, R., & DeSouza, J. F. X. (2017). Experience-dependent modulation of alpha and beta during action observation and motor imagery. *BMC Neuroscience*, *18*(1), 28. https://doi.org/10.1186/s12868-017-0349-0

Diekfuss, J. A., Grooms, D. R., Nissen, K. S., Schneider, D. K., Foss, K. D. B., Thomas, S., Bonnette, S., Dudley, J. A., Yuan, W., Reddington, D. L., Ellis, J. D., Leach, J., Gordon, M., Lindsey, C., Rushford, K., Shafer, C., & Myer, G. D. (2020). Alterations in knee sensorimotor brain functional connectivity contributes to ACL injury in male high-school football players: a prospective neuroimaging analysis. *Brazilian Journal of Physical Therapy*, *24*(5), 415–423. https://doi.org/10.1016/j.bjpt.2019.07.004

Diekfuss, J. A., Grooms, D. R., Yuan, W., Dudley, J., Barber Foss, K. D., Thomas, S., Ellis, J. D., Schneider, D. K., Leach, J., Bonnette, S., & Myer, G. D. (2019). Does brain functional connectivity contribute to musculoskeletal injury? A preliminary prospective analysis of a neural biomarker of ACL injury risk. *Journal of Science and Medicine in Sport*, *22*(2), 169–174. https://doi.org/10.1016/j.jsams.2018.07.004

Drew, M. K., Raysmith, B. P., & Charlton, P. C. (2017). Injuries impair the chance of successful performance by sportspeople: a systematic review. *British Journal of Sports Medicine*, *51*(16), 1209–1214. https://doi.org/10.1136/bjsports-2016-096731

Edwards, L. L., King, E. M., Buetefisch, C. M., & Borich, M. R. (2019). Putting the "Sensory" Into Sensorimotor Control: The Role of Sensorimotor Integration in Goal-Directed Hand Movements After Stroke. *Frontiers in Integrative Neuroscience*, *13*. https://doi.org/10.3389/fnint.2019.00016

Eirale, C., Tol, J. L., Farooq, A., Smiley, F., & Chalabi, H. (2013). Low injury rate strongly correlates with team success in Qatari professional football. *British Journal of Sports Medicine*, *47*(12), 807–808. https://doi.org/10.1136/bjsports-2012-091040

Ekstrand, J., Bengtsson, H., Waldén, M., Davison, M., Khan, K. M., & Hägglund, M. (2023). Hamstring injury rates have increased during recent seasons and now constitute 24% of all injuries in men's professional football: the UEFA Elite Club Injury Study from 2001/02 to 2021/22. *British Journal of Sports Medicine*, *57*(5), 292–298. https://doi.org/10.1136/bjsports-2021-105407

Ferrillo, F., Beelke, M., & Nobili, L. (2000). Sleep EEG synchronization mechanisms and activation of interictal epileptic spikes. *Clinical Neurophysiology*, *111*, S65–S73. https://doi.org/10.1016/S1388-2457(00)00404-1

Fine, E. J., Ionita, C. C., & Lohr, L. (2002). The history of the development of the cerebellar examination. *Semin. Neurol.*, *22*(4), 375–384.

Fingelkurts, A. A., Fingelkurts, A. A., & Kähkönen, S. (2005). Functional connectivity in the brain–is it an elusive concept? *Neurosci. Biobehav. Rev.*, *28*(8), 827–836.

Fink, A., Rominger, C., Benedek, M., Perchtold, C. M., Papousek, I., Weiss, E. M., Seidel, A., & Memmert, D. (2018). EEG alpha activity during imagining creative moves in soccer decision-making situations. *Neuropsychologia*, *114*, 118–124. https://doi.org/10.1016/j.neuropsychologia.2018.04.025

Fortune, B. C., Pretty, C. G., Cameron, C. J., McKenzie, L. R., Chatfield, L. T., & Hayes, M. P. (2021). Electrode–skin impedance imbalance measured in the frequency domain. *Biomedical Signal Processing and Control*, *63*, 102202. https://doi.org/10.1016/j.bspc.2020.102202

Foxe, J. J., & Snyder, A. C. (2011). The Role of Alpha-Band Brain Oscillations as a Sensory Suppression Mechanism during Selective Attention. *Frontiers in Psychology*, *2*. https://doi.org/10.3389/fpsyg.2011.00154

Freund, H. J. (2001). The parietal lobe as a sensorimotor interface: a perspective from clinical and neuroimaging data. *Neuroimage*, *14*(1 Pt 2), S142–6.

Fuller, C. W., Ekstrand, J., Junge, A., Andersen, T. E., Bahr, R., Dvorak, J., H??gglund, M., McCrory, P., & Meeuwisse, W. H. (2006). Consensus Statement on Injury Definitions and Data Collection Procedures in Studies of Football (Soccer) Injuries. *Clinical Journal of Sport Medicine*, *16*(2), 97–106. https://doi.org/10.1097/00042752-200603000-00003

Fuster. (2014). *The Prefrontal Cortex* (J. Fuster, Ed.; 4th ed.). Academic Press.

Fyfe, J. J., Opar, D. A., Williams, M. D., & Shield, A. J. (2013). The role of neuromuscular inhibition in hamstring strain injury recurrence. *Journal of Electromyography and Kinesiology*, *23*(3), 523–530. https://doi.org/10.1016/j.jelekin.2012.12.006

Gabard-Durnam, L. J., Mendez Leal, A. S., Wilkinson, C. L., & Levin, A. R. (2018). The Harvard Automated Processing Pipeline for Electroencephalography (HAPPE): Standardized Processing Software for Developmental and High-Artifact Data. *Frontiers in Neuroscience*, *12*. https://doi.org/10.3389/fnins.2018.00097

Gabbe, B. J., Finch, C. F., Bennell, K. L., & Wajswelner, H. (2003). How valid is a self reported 12 month sports injury history?: Figure 1. *British Journal of Sports Medicine*, *37*(6), 545–547. https://doi.org/10.1136/bjsm.37.6.545

Goncharova, I. I., McFarland, D. J., Vaughan, T. M., & Wolpaw, J. R. (2003). EMG contamination of EEG: spectral and topographical characteristics. *Clin. Neurophysiol.*, *114*(9), 1580–1593.

Gong, G., He, Y., Concha, L., Lebel, C., Gross, D. W., Evans, A. C., & Beaulieu, C. (2009). Mapping Anatomical Connectivity Patterns of Human Cerebral Cortex Using In Vivo Diffusion Tensor Imaging Tractography. *Cerebral Cortex*, *19*(3), 524–536. https://doi.org/10.1093/cercor/bhn102

Graven-Nielsen, T., & Arendt-Nielsen, L. (2010). Assessment of mechanisms in localized and widespread musculoskeletal pain. *Nature Reviews Rheumatology*, *6*(10), 599–606. https://doi.org/10.1038/nrrheum.2010.107

Habibzadeh Tonekabony Shad, E., Molinas, M., & Ytterdal, T. (2020). Impedance and Noise of Passive and Active Dry EEG Electrodes: A Review. *IEEE Sensors Journal*, *20*(24), 14565–14577. https://doi.org/10.1109/JSEN.2020.3012394

Hägglund, M., Waldén, M., Magnusson, H., Kristenson, K., Bengtsson, H., & Ekstrand, J. (2013). Injuries affect team performance negatively in professional football: an 11-year follow-up of the UEFA Champions League injury study. *British Journal of Sports Medicine*, *47*(12), 738–742. https://doi.org/10.1136/bjsports-2013-092215

Haines, D. E., & Terrell, A. C. (2018). Orientation to the structure and imaging of the central nervous system. In *Fundamental Neuroscience for Basic and Clinical Applications* (pp. 3–14.e1). Elsevier.

Hamal, A. Q., & Rehman, A. W. B. A. (2013, December). Artifact processing of epileptic EEG signals: An overview of different types of artifacts. *2013 International Conference on Advanced Computer Science and Technologies*.

Hammond, C. (2015). Ionic gradients, membrane potential and ionic currents. In *Cellular and Molecular Neurophysiology* (pp. 39–54). Elsevier. https://doi.org/10.1016/B978-0-12-397032-9.00003-0

Heiderscheit, B. C., Sherry, M. A., Silder, A., Chumanov, E. S., & Thelen, D. G. (2010). Hamstring Strain Injuries: Recommendations for Diagnosis, Rehabilitation, and Injury Prevention. *Journal of Orthopaedic & Sports Physical Therapy*, *40*(2), 67–81. https://doi.org/10.2519/jospt.2010.3047

Hodgkin, A. L., & Huxley, A. F. (1952). A quantitative description of membrane current and its application to conduction and excitation in nerve. *The Journal of Physiology*, *117*(4), 500–544. https://doi.org/10.1113/jphysiol.1952.sp004764

Humphrey, D. R., & Schmidt, E. M. (n.d.). Extracellular Single-Unit Recording Methods. In *Neurophysiological Techniques, II* (pp. 1–64). Humana Press. https://doi.org/10.1385/0-89603-185-3:1

Ismail, L. E., & Karwowski, W. (2020). A Graph Theory-Based Modeling of Functional Brain Connectivity Based on EEG: A Systematic Review in the Context of Neuroergonomics. *IEEE Access*, *8*, 155103–155135. https://doi.org/10.1109/ACCESS.2020.3018995

Jiang, X., Bian, G.-B., & Tian, Z. (2019). Removal of artifacts from EEG signals: A review. *Sensors (Basel)*, *19*(5), 987.

Jokela, A., Valle, X., Kosola, J., Rodas, G., Til, L., Burova, M., Pleshkov, P., Andersson, H., Pasta, G., Manetti, P., Lupón, G., Pruna, R., García-Romero-Pérez, A., & Lempainen, L. (2023). Mechanisms of Hamstring Injury in Professional Soccer Players: Video Analysis and Magnetic Resonance Imaging Findings. *Clinical Journal of Sport Medicine*, *33*(3), 217–224. https://doi.org/10.1097/JSM.0000000000001109

Joynt, R. (2024). brainstem. In *Encyclopedia Britannica*.

Junghöfer, M., Elbert, T., Tucker, D. M., & Braun, C. (1999). The polar average reference effect: a bias in estimating the head surface integral in EEG recording. *Clin. Neurophysiol.*, *110*(6), 1149–1155.

Jurcak, V., Tsuzuki, D., & Dan, I. (2007). 10/20, 10/10, and 10/5 systems revisited: Their validity as relative head-surface-based positioning systems. *NeuroImage*, *34*(4), 1600–1611. https://doi.org/10.1016/j.neuroimage.2006.09.024

Kamijo, K., Nishihira, Y., Higashiura, T., & Kuroiwa, K. (2007). The interactive effect of exercise intensity and task difficulty on human cognitive processing. *International Journal of Psychophysiology*, *65*(2), 114–121. https://doi.org/10.1016/j.ijpsycho.2007.04.001

Kandel, E. R., Schwartz, J. H., Jessell, T. M., & Siegelbaum S and Hudspeth, J. (2013). *Principles Neural Science*. McGraw-Hill.

Kappenman, E. S., & Luck, S. J. (2010). The effects of electrode impedance on data quality and statistical significance in ERP recordings. *Psychophysiology*, *47*(5), 888–904.

Kaya, İ. (2022). *A Brief Summary of EEG Artifact Handling*. https://doi.org/10.5772/intechopen.99127

Khoa, W., Long, G., & Eng, B. (2013). *STUDY OF THE CHARACTERISTICS OF SCALP ELECTROENCEPHALOGRAPHY SENSING*.

Kim, S.-P. (2018). Preprocessing of EEG. In *Biological and Medical Physics, Biomedical Engineering* (pp. 15–33). Springer Singapore.

Kirmizi-Alsan, E., Bayraktaroglu, Z., Gurvit Hakan and Keskin, Y. H., Emre, M., & Demiralp, T. (2006). Comparative analysis of event-related potentials during Go/NoGo and CPT:

decomposition of electrophysiological markers of response inhibition and sustained attention. *Brain Res.*, *1104*(1), 114–128.

Kirschstein, T., & Köhling, R. (2009). What is the source of the EEG? *Clin. EEG Neurosci.*, *40*(3), 146–149.

Kisley, M. A., & Cornwell, Z. M. (2006). Gamma beta neural activity evoked during sensory gating paradigm: effects auditory, somatosensory cross-modal stimulation. *Clinical Neurophysiology*, *117*(11), 2549–2563.

Kolb, B., & Whishaw, I. Q. (2015). *Fundamentals Human Neuropsychology*. Worth Publishers.

Kulaichev, A. P. (2016). Optimal choice of a reference electrode for EEG recording. *Moscow University Biological Sciences Bulletin*, *71*(3), 145–150. https://doi.org/10.3103/S0096392516030068

Latora, V., & Marchiori, M. (2001). Efficient Behavior of Small-World Networks. *Physical Review Letters*, *87*(19), 198701. https://doi.org/10.1103/PhysRevLett.87.198701

Lee, K. J., Park, C., & Lee, B. (2015, October). Elimination of ECG artifacts from a single-channel EEG using sparse derivative method. *2015 IEEE International Conference on Systems, Man, And*.

Liao, X., Vasilakos, A. V., & He, Y. (2017). Small-world human brain networks: Perspectives and challenges. *Neuroscience & Biobehavioral Reviews*, *77*, 286–300. https://doi.org/10.1016/j.neubiorev.2017.03.018

Liu, Z., Zhang, Y., Yan, H., Bai, L., Dai, R., Wei, W., Zhong, C., Xue, T., Wang, H., Feng, Y., You, Y., Zhang, X., & Tian, J. (2012). Altered topological patterns of brain networks in mild cognitive impairment and Alzheimer's disease: A resting-state fMRI study. *Psychiatry Research: Neuroimaging*, *202*(2), 118–125. https://doi.org/10.1016/j.pscychresns.2012.03.002

Lopez, K. L., Monachino, A. D., Morales, S., Leach, S. C., Bowers, M. E., & Gabard-Durnam, L. J. (2022). HAPPILEE: HAPPE In Low Electrode Electroencephalography, a standardized pre-processing software for lower density recordings. *NeuroImage*, *260*, 119390. https://doi.org/10.1016/j.neuroimage.2022.119390

Lopez-Gordo, M., Sanchez-Morillo, D., & Valle, F. (2014). Dry EEG Electrodes. *Sensors*, *14*(7), 12847–12870. https://doi.org/10.3390/s140712847

Martin, R. L., Cibulka, M. T., Bolgla, L. A., Koc, T. A., Loudon, J. K., Manske, R. C., Weiss, L., Christoforetti, J. J., & Heiderscheit, B. C. (2022). Hamstring Strain Injury in Athletes. *Journal of Orthopaedic & Sports Physical Therapy*, *52*(3), CPG1–CPG44. https://doi.org/10.2519/jospt.2022.0301

Moroni, F., Nobili, L., De Carli, F., Massimini, M., Francione, S., Marzano, C., Proserpio, P., Cipolli, C., De Gennaro, L., & Ferrara, M. (2012). Slow EEG rhythms and inter-hemispheric synchronization across sleep and wakefulness in the human hippocampus. *NeuroImage*, *60*(1), 497–504. https://doi.org/10.1016/j.neuroimage.2011.11.093

Moukhaiber, N., Summers, S. J., Opar, D., Imam, J., Thomson, D., Chang, W.-J., Andary, T., & Cavaleri, R. (2023). The Effect of Theta Burst Stimulation Over the Primary Motor Cortex on Experimental Hamstring Pain: A Randomized, Controlled Study. *The Journal of Pain*, *24*(4), 593–604. https://doi.org/10.1016/j.jpain.2022.11.013

Neuman, M. (1998). *Medical instrumentation application design*. J. Wiley Sons.

Neuper, C., & Pfurtscheller, G. (2001). Event-related dynamics of cortical rhythms: frequency-specific features and functional correlates. *International Journal of Psychophysiology*, *43*(1), 41–58. https://doi.org/10.1016/S0167-8760(01)00178-7

Nieto Torrejón, L., Martínez-Serrano, A., Villalón, J. M., & Alcaraz, P. E. (2024). Economic impact of muscle injury rate and hamstring strain injuries in professional football clubs. Evidence from LaLiga. *PLOS ONE*, *19*(6), e0301498. https://doi.org/10.1371/journal.pone.0301498

Oostenveld, R., & Praamstra, P. (2001). The five percent electrode system for high-resolution EEG and ERP measurements. *Clinical Neurophysiology*, *112*(4), 713–719. https://doi.org/10.1016/S1388-2457(00)00527-7

Opar, D. A., Williams, M. D., & Shield, A. J. (2012). Hamstring Strain Injuries. *Sports Medicine*, *42*(3), 209–226. https://doi.org/10.2165/11594800-000000000-00000

O'Sullivan, M., Temko, A., Bocchino, A., O'Mahony, C., Boylan, G., & Popovici, E. (2019). Analysis of a low-cost EEG monitoring system and dry electrodes toward clinical use in the neonatal ICU. *Sensors (Basel)*, *19*(11), 2637.

Pape, A.-A., & Siegel, M. (2016). Motor cortex activity predicts response alternation during sensorimotor decisions. *Nature Communications*, *7*(1), 13098. https://doi.org/10.1038/ncomms13098

Park, H.-J., & Friston, K. (2013). Structural and Functional Brain Networks: From Connections to Cognition. *Science*, *342*(6158). https://doi.org/10.1126/science.1238411

Paton, B. M., Read, P., van Dyk, N., Wilson, M. G., Pollock, N., Court, N., Giakoumis, M., Head, P., Kayani, B., Kelly, S., Kerkhoffs, G. M. M. J., Moore, J., Moriarty, P., Murphy, S., Plastow, R., Stirling, B., Tulloch, L., Wood, D., & Haddad, F. (2023). London International Consensus and Delphi study on hamstring injuries part 3: rehabilitation, running and return to sport. *British Journal of Sports Medicine*, *57*(5), 278–291. https://doi.org/10.1136/bjsports-2021-105384

Picton, T. W., Bentin, S., Berg, P., Donchin, E., Hillyard, S. A., Johnson, R., Miller, G. A., Ritter, W., Ruchkin, D. S., Rugg, M. D., & Taylor, M. J. (2000). Guidelines for using human event-related potentials to study cognition: recording standards and publication criteria. *Psychophysiology*, *37*(2), 127–152.

Raufi, B., & Longo, L. (2022). An Evaluation of the EEG Alpha-to-Theta and Theta-to-Alpha Band Ratios as Indexes of Mental Workload. *Frontiers in Neuroinformatics*, *16*. https://doi.org/10.3389/fninf.2022.861967

Richardson, J. T. E. (2011). Eta squared and partial eta squared as measures of effect size in educational research. *Educational Research Review*, *6*(2), 135–147. https://doi.org/10.1016/j.edurev.2010.12.001

Røksund, O. D., Kristoffersen, M., Bogen, B. E., Wisnes, A., Engeseth, M. S., Nilsen, A.-K., Iversen, V. V., Mæland, S., & Gundersen, H. (2017). Higher Drop in Speed during a Repeated Sprint Test in Soccer Players Reporting Former Hamstring Strain Injury. *Frontiers in Physiology*, *8*. https://doi.org/10.3389/fphys.2017.00025

Rosenblum, M. G., Pikovsky, A. S., & Kurths, J. (1996). Phase synchronization of chaotic oscillators. *Phys. Rev. Lett.*, *76*(11), 1804–1807.

Rosenfeld, J. P. (2000). Theoretical Implications of EEG Reference Choice and Related Methodology Issues. *Journal of Neurotherapy*, *4*(2), 77–87. https://doi.org/10.1300/J184v04n02_08

Roussiez, V., & Van Cant, J. (2019). Predisposing factors to hamstring neuromuscular deficits—implications for prevention and rehabilitation of hamstring strain injuries: a narrative review. *Physical Therapy Reviews*, *24*(3–4), 125–133. https://doi.org/10.1080/10833196.2019.1616375

Royer, J., Bernhardt, B. C., Larivière, S., Gleichgerrcht, E., Vorderwülbecke, B. J., Vulliémoz, S., & Bonilha, L. (2022). Epilepsy and brain network hubs. *Epilepsia*, *63*(3), 537–550. https://doi.org/10.1111/epi.17171

Schuermans, J., Van Tiggelen, D., Danneels, L., & Witvrouw, E. (2014). Biceps femoris and semitendinosus—teammates or competitors? New insights into hamstring injury mechanisms in male football players: a muscle functional MRI study. *British Journal of Sports Medicine*, *48*(22), 1599–1606. https://doi.org/10.1136/bjsports-2014-094017

Shaw, E. P., Rietschel, J. C., Shuggi, I. M., Xu, Y., Chen, S., Miller, M. W., Hatfield, B. D., & Gentili, R. J. (2019). Cerebral cortical networking for mental workload assessment under various demands during dual-task walking. *Experimental Brain Research*, *237*(9), 2279–2295. https://doi.org/10.1007/s00221-019-05550-x

Simon, S. R., Meunier, M., Piettre, L., Berardi, A. M., Segebarth, C. M., & Boussaoud, D. (2002). Spatial attention and memory versus motor preparation: premotor cortex involvement as revealed by fMRI. *J. Neurophysiol.*, *88*(4), 2047–2057.

Stam, C. J., Nolte, G., & Daffertshofer, A. (2007). Phase lag index: assessment of functional connectivity from multi channel EEG and MEG with diminished bias from common sources. *Hum. Brain Mapp.*, *28*(11), 1178–1193.

Summers, S. J., Chalmers, K. J., Wallwork, S. B., Leake, H. B., & Moseley, G. L. (2021). Interrogating cortical representations in elite athletes with persistent posterior thigh pain – New targets for intervention? *Journal of Science and Medicine in Sport*, *24*(2), 135–140. https://doi.org/10.1016/j.jsams.2020.07.003

Tadel, F., Baillet, S., Mosher, J. C., Pantazis, D., & Leahy, R. M. (2011). Brainstorm: A User-Friendly Application for MEG/EEG Analysis. *Computational Intelligence and Neuroscience*, *2011*, 1–13. https://doi.org/10.1155/2011/879716

Tanner, D., Morgan-Short, K., & Luck, S. J. (2015). How inappropriate high-pass filters can produce artifactual effects and incorrect conclusions in ERP studies of language and cognition. *Psychophysiology*, *52*(8), 997–1009.

Thilaga, M., Ramasamy, V., Nadarajan, R., & Nandagopal, D. (2018). Shortest path based network analysis to characterize cognitive load states of human brain using EEG based functional brain networks. *Journal of Integrative Neuroscience*, *17*(2), 253–275. https://doi.org/10.3233/JIN-170049

Tim Mullen. (2012). *Mullen, T. (2012). CleanLine EEGLAB plugin.* . Neuroimaging Informatics Toolsand Resources Clearinghouse (NITRC).

Ulanov, M., & Shtyrov, Y. (2022). Oscillatory beta/alpha band modulations: A potential biomarker of functional language and motor recovery in chronic stroke? *Frontiers in Human Neuroscience*, *16*. https://doi.org/10.3389/fnhum.2022.940845

Urigüen, J. A., & Garcia-Zapirain, B. (2015). EEG artifact removal—state-of-the-art and guidelines. *J. Neural Eng.*, *12*(3), 31001.

Usakli, A. B. (2010). Improvement of EEG Signal Acquisition: An Electrical Aspect for State of the Art of Front End. *Computational Intelligence and Neuroscience*, *2010*, 1–7. https://doi.org/10.1155/2010/630649

Vinck, M., Oostenveld, R., van Wingerden, M., Battaglia, F., & Pennartz, C. M. A. (2011). An improved index of phase-synchronization for electrophysiological data in the presence of volume-conduction, noise and sample-size bias. *NeuroImage*, *55*(4), 1548–1565. https://doi.org/10.1016/j.neuroimage.2011.01.055

Vojkan Mihahlovic, & Garcia-Molina Gary. (2012). TO WHAT EXTENT CAN DRY AND WATER-BASED EEG ELECTRODES REPLACE CONDUCTIVE GEL ONES? - A Steady State Visual Evoked Potential Brain-computer Interface Case Study. *Proceedings of the International Conference on Biomedical Electronics and Devices*, 14–26. https://doi.org/10.5220/0003726000140026

Wallstrom, G. L., Kass, R. E., Miller, A., Cohn, J. F., & Fox, N. A. (2004). Automatic correction of ocular artifacts in the EEG: a comparison of regression-based and component-based methods. *Int. J. Psychophysiol.*, *53*(2), 105–119.

Wasserman, S., & Faust, K. (1994). *Social Network Analysis*. Cambridge University Press. https://doi.org/10.1017/CBO9780511815478

Widmaier, E., Raff, H., & Strang, K. (2004). *Vander's Human Physiology: mechanisms body function*. McGraw-Hill Higher Education.

Widmann, A., Schröger, E., & Maess, B. (2015). Digital filter design for electrophysiological data–a practical approach. *J. Neurosci. Methods*, *250*, 34–46.

Wolpert, D. M., Goodbody, S. J., & Husain, M. (1998). Maintaining internal representations: the role of the human superior parietal lobe. *Nat. Neurosci.*, *1*(6), 529–533.

Wong, A. L., Haith, A. M., & Krakauer, J. W. (2015). Motor planning. *Neuroscientist*, *21*(4), 385–398.

Yang, L., Liu, Q., Zhang, Z., Gan, L., Zhang, Y., & Wu, J. (2022). Materials for Dry Electrodes for the Electroencephalography: Advances, Challenges, Perspectives. *Advanced Materials Technologies*, *7*(3). https://doi.org/10.1002/admt.202100612

Yao, D. (2001). A method to standardize a reference of scalp EEG recordings to a point at infinity. *Physiol. Meas.*, *22*(4), 693–711.

Yuan, H., Li, Y., Yang, J., Li, H., Yang, Q., Guo, C., Zhu, S., & Shu, X. (2021). State of the Art of Non-Invasive Electrode Materials for Brain–Computer Interface. *Micromachines*, *12*(12), 1521. https://doi.org/10.3390/mi12121521

Zhang, X., Su, W., Ruan, B., & Zang, Y. (2022). Alterations in Cortical Activation among Soccer Athletes with Chronic Ankle Instability during Drop-Jump Landing: A Preliminary Study. *Brain Sciences*, *12*(5), 664. https://doi.org/10.3390/brainsci12050664

APPENDIX

A.1. Some other results from the alpha frequency band.

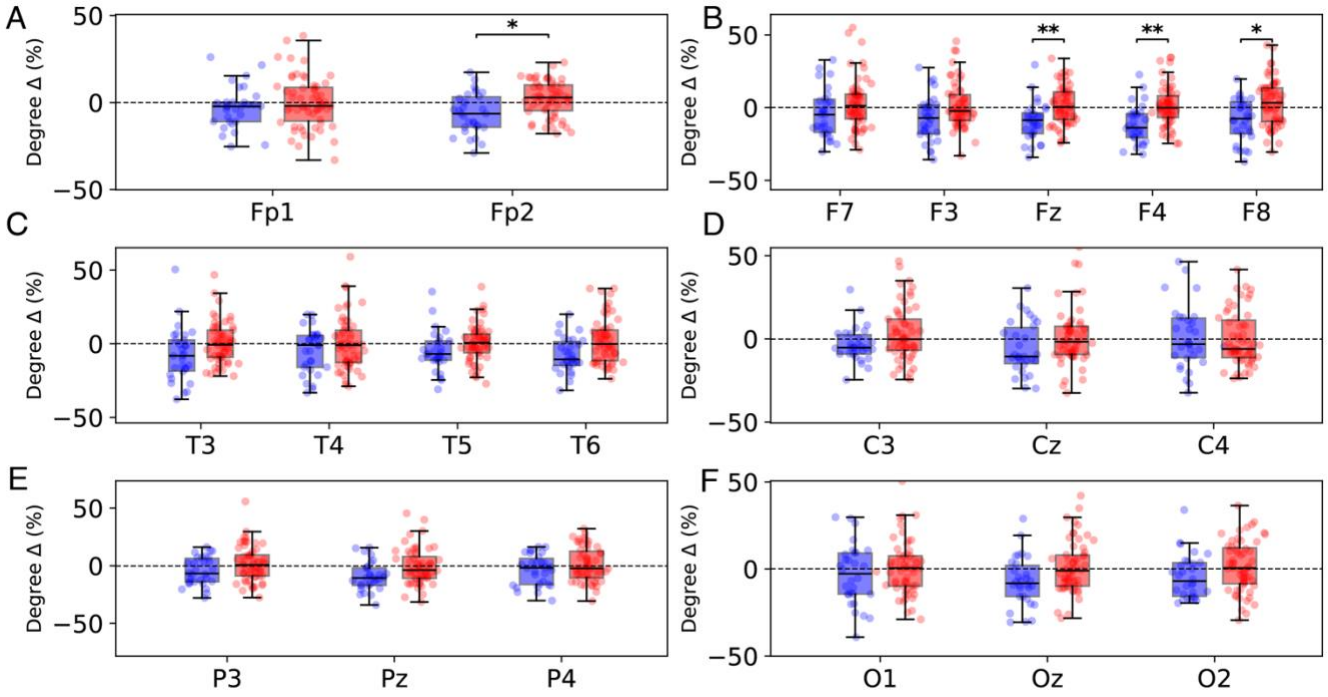

Figure A1. Group comparison of alpha FC percent change for all nodes in the network. Boxplots comparing the percent degree change from individual nodes from each respective network (Blue = injured, Red = control). (A) Prefrontal, (B) frontal, (C) temporal, (D) central, (E) parietal and (F) occipital.

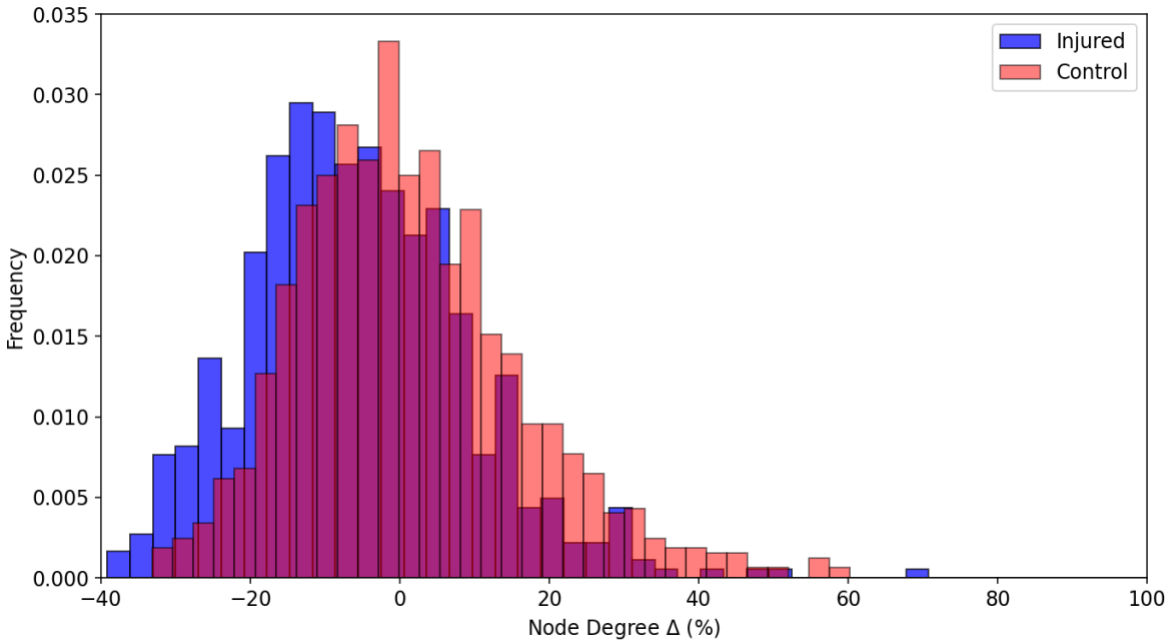

Figure A2. Histogram of node degree change (%). Mann-Whitney U test for comparing distributions results: effect size *r=0.26* (small), *p-value < 0.0001*

A.2. Results from theta and beta frequency bands.

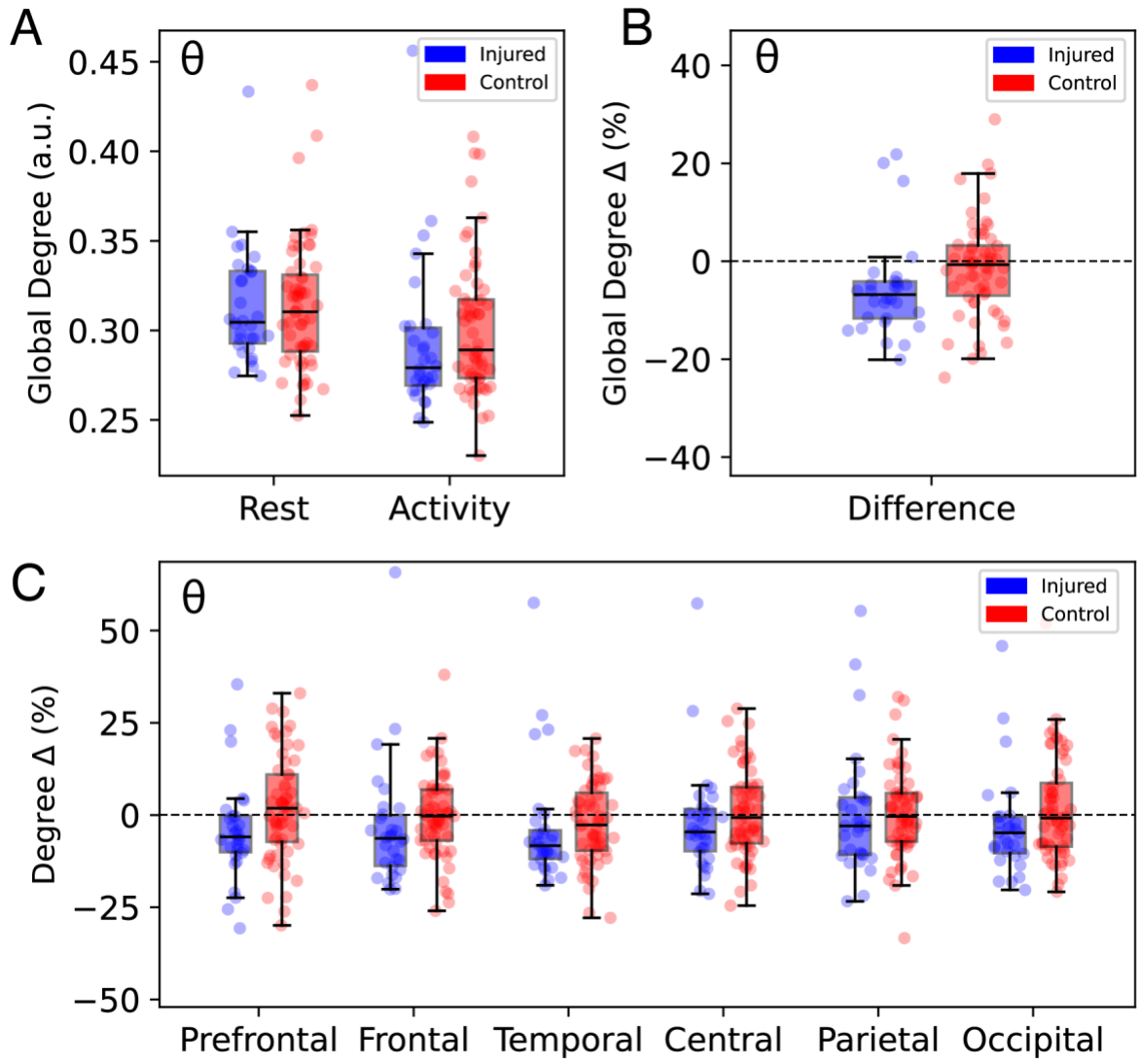

Figure A3. Group comparisons of brain FC at theta. (A) Boxplot comparing the global degree between activity and rest epochs for both injured (blue) and control (red) groups. (B) Boxplot comparing the percent change in global degree when transitioning from rest to activity for both groups. (C) Boxplot comparing the percent change in local degree for each of the 6 networks for both groups.

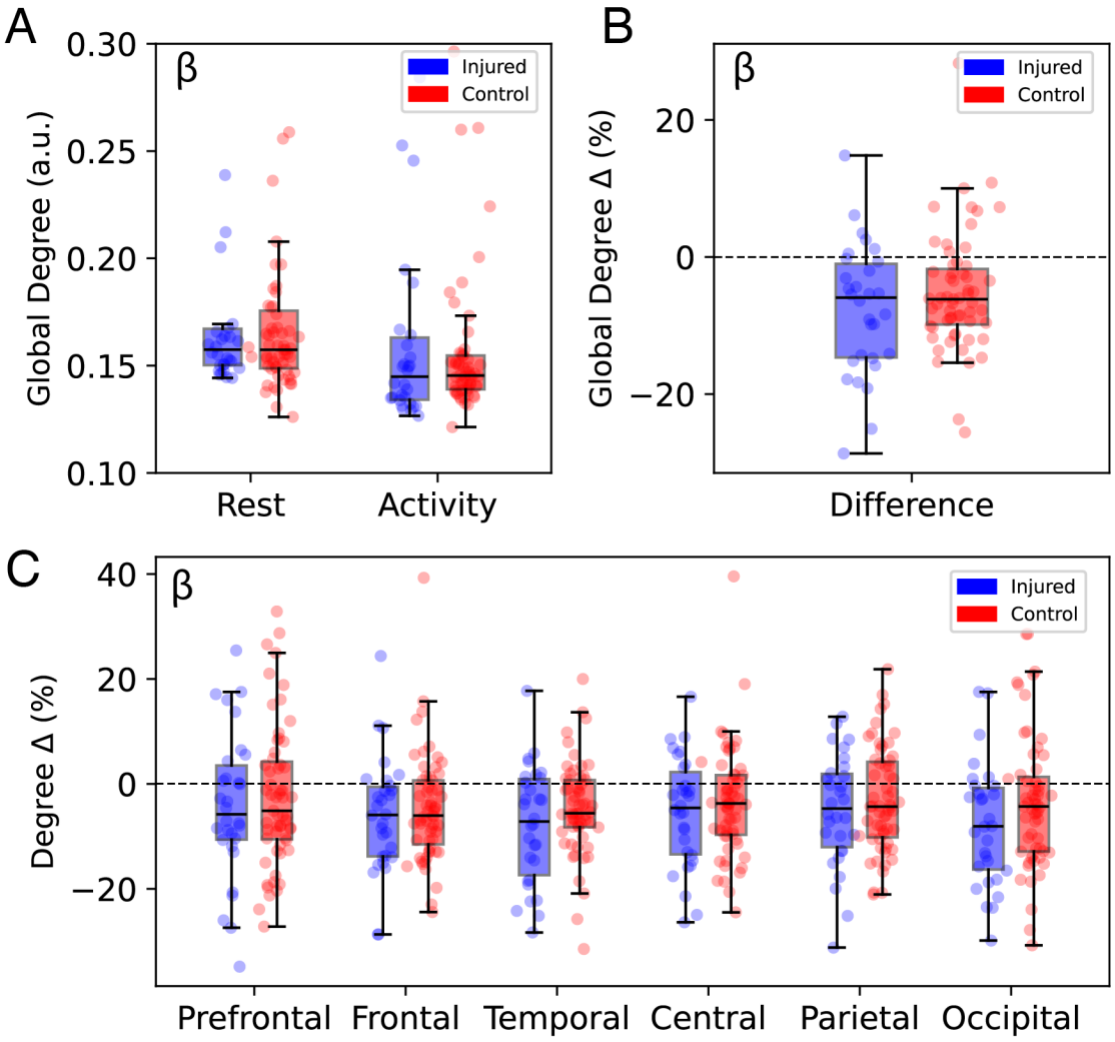

Figure A4. Group comparisons of brain FC at beta. (A) Boxplot comparing the global degree between activity and rest epochs for both injured (blue) and control (red) groups. (B) Boxplot comparing the percent change in global degree when transitioning from rest to activity for both groups. (C) Boxplot comparing the percent change in local degree for each of the 6 networks for both groups.

Table A1. Results from the partial correlation analysis of injury parameters and network degree changes at theta band. Each cell represents the correlation results in the format: [r-value, CI95%, p-value]. Bold cells contain significant p-values ($p<0.05$).

	Days away due to injury	Days since injury	Severity Score	Severity Index
Global	[-0.25, (-0.56, 0.12), 0.71]	[-0.13, (-0.47, 0.24), 1]	[-0.45, (-0.69, -0.1), 0.054]	[-0.15, (-0.48, 0.22), 1]
Prefrontal	[-0.27, (-0.57, 0.1), 1]	[-0.16, (-0.49, 0.21), 1]	[-0.47, (-0.71, -0.14), 0.197]	[-0.14, (-0.48, 0.23), 1]
Frontal	[-0.12, (-0.46, 0.25), 1]	[-0.07, (-0.42, 0.29), 1]	[-0.32, (-0.61, 0.05), 1]	[-0.1, (-0.44, 0.27), 1]
Parietal	[-0.33, (-0.62, 0.03), 1]	[0.04, (-0.33, 0.39), 1]	[-0.44, (-0.69, -0.09), 0.36]	[-0.19, (-0.51, 0.18), 1]
Central	[-0.08, (-0.43, 0.29), 1]	[-0.1, (-0.44, 0.27), 1]	[-0.31, (-0.6, 0.06), 1]	[-0.17, (-0.5, 0.2), 1]
Temporal	[-0.24, (-0.55, 0.13), 1]	[-0.16, (-0.49, 0.21), 1]	[-0.38, (-0.65, -0.03), 0.89]	[-0.05, (-0.41, 0.31), 1]
Occipital	[-0.23, (-0.55, 0.14), 1]	[-0.15, (-0.49, 0.22), 1]	[-0.41, (-0.67, -0.06), 0.59]	[-0.12, (-0.46, 0.25), 1]

Table A2. Results from the partial correlation analysis of injury parameters and network degree changes at beta band. Each cell represents the correlation results in the format: [r-value, CI95%, p-value]. Bold cells contain significant p-values ($p<0.05$).

	Days away due to injury	Days since injury	Severity Score	Severity Index
Global	[0.12, (-0.25, 0.46), 1]	[-0.02, (-0.38, 0.34), 1]	[-0.1, (-0.45, 0.27), 1]	[-0.17, (-0.5, 0.2), 1]
Prefrontal	[0.19, (-0.18, 0.51), 1]	[0.03, (-0.34, 0.38), 1]	[0.04, (-0.32, 0.4), 1]	[-0.04, (-0.4, 0.32), 1]
Frontal	[0.01, (-0.36, 0.37), 1]	[0.07, (-0.3, 0.42), 1]	[-0.22, (-0.54, 0.15), 1]	[-0.24, (-0.55, 0.13), 1]
Parietal	[-0.01, (-0.37, 0.35), 1]	[-0.12, (-0.46, 0.25), 1]	[-0.11, (-0.45, 0.26), 1]	[-0.24, (-0.55, 0.13), 1]
Central	[0.08, (-0.28, 0.43), 1]	[-0.05, (-0.4, 0.32), 1]	[-0.24, (-0.55, 0.13), 1]	[-0.16, (-0.49, 0.21), 1]
Temporal	[0.14, (-0.23, 0.48), 1]	[-0.16, (-0.49, 0.22), 1]	[-0.1, (-0.44, 0.27), 1]	[-0.09, (-0.43, 0.28), 1]
Occipital	[0.09, (-0.28, 0.43), 1]	[0.08, (-0.29, 0.43), 1]	[-0.07, (-0.42, 0.3), 1]	[-0.2, (-0.52, 0.17), 1]